Check for updates

ADVANCED FUNCTIONAL MATERIALS
www.afm-journal.de

Microstructuring of Thermoresponsive Biofunctional Hydrogels by Multiphoton Photocrosslinking

Yevhenii M. Morozov, Fiona Wiesner (née Diehl), Jonas J. Grün, Matthias Pertiller, Stefan Fossati, Katharina Schmidt, Nestor Gisbert Quilis, Claudia Gusenbauer, Barbara Zbiral, Jose Luis Toca-Herrera, Sven Klees, Clinton Richard Victor Thiagarajan, Ulrich Jonas,* and Jakub Dostalek**

A pioneering method is reported for creating thermoresponsive biofunctional hydrogel microstructures using maskless multiphoton lithography. Departing from conventional multiphoton-triggered polymerization-based techniques, this approach relies on simultaneous photocrosslinking and attachment of already pre-synthesized polymer chains onto solid substrates. The method allows improving control over polymer network characteristics and enables facile integration of additional functionalities through postmodification with biomolecules at specific sites. Exploring two distinct benzophenone- and anthraquinone-based photocrosslinkers incorporated into specially designed poly(*N*-isopropyl acrylamide)-based co- and terpolymers, the photocrosslinking efficacy is scrutinized with the use of a custom femtosecond near-infrared laser lithographer. Comprehensive characterization via surface plasmon resonance imaging, atomic force microscopy, and optical fluorescence microscopy reveals swelling behavior and demonstrates postmodification feasibility. Notably, within a specific range of multiphoton photocrosslinking parameters, the surface-attached microstructures exhibit a quasiperiodic topography akin to wrinkle-pattern formation. Leveraging the capabilities of established multiphoton lithographer systems that offer fast pattern writing with high resolution, this approach holds great promise for the versatile fabrication of multifunctional 3D micro- and nanostructures. Such tailored responsive biofunctional materials with spatial control over composition, swelling behavior, and postmodification are particularly attractive in the areas of bioanalytical and biomedical technologies.

1. Introduction

Polymers responsive to a variety of stimuli such as temperature,[1] pH,[2] mechanical force,[3] chemical species,[4] and electric/magnetic field[5,6] have already become essential building blocks serving in the design of advanced functional materials.[7–10] Among these, poly(*N*-isopropyl acrylamide) (pNIPAAm) is one of the most studied responsive polymers. This polymer can be toggled between a coil and globule state in an aqueous solution by changing the temperature below or above the cloud point temperature that occurs close to the human body temperature,[1,11–13] which is a result of its lower critical solution temperature (LCST) characteristics. This material is commonly used for the preparation of networks that act as thermoresponsive hydrogels in the form of free-standing or surface-attached elements. Such pNIPAAm-based structures are typically prepared by UV-triggered photopolymerization in conjunction with casting in miniature molds.[14] In another route, similar photochemistry is exploited in stereolithography by scanning a UV beam,[15] or in shadow mask lithography[16] for the

Y. M. Morozov
Center for Health & Bioresources
AIT-Austrian Institute of Technology
Giefinggasse 4, Vienna 1210, Austria
E-mail: Yevhenii.Morozov@ait.ac.at

The ORCID identification number(s) for the author(s) of this article can be found under https://doi.org/10.1002/adfm.202315578

© 2024 The Authors. Advanced Functional Materials published by Wiley-VCH GmbH. This is an open access article under the terms of the Creative Commons Attribution License, which permits use, distribution and reproduction in any medium, provided the original work is properly cited.

DOI: 10.1002/adfm.202315578

F. Wiesner (née Diehl), J. J. Grün, S. Klees, C. R. V. Thiagarajan, U. Jonas
Macromolecular Chemistry
Department of Chemistry and Biology
University of Siegen
Adolf Reichwein-Straße 2, 57076 Siegen, Germany
E-mail: jonas@chemie.uni-siegen.de

M. Pertiller, K. Schmidt, J. Dostalek
LiST-Life Sciences Technology
Danube Private University
Viktor-Kaplan-Straße 2, Wiener Neustadt 2700, Austria
E-mail: dostalek@fzu.cz

16163028, 2024, 26, Downloaded from https://onlinelibrary.wiley.com/doi/10.1002/adfm.202315578 by Readcube (Labtiva Inc.), Wiley Online Library on [01/07/2024]. See the Terms and Conditions (https://onlinelibrary.wiley.com/terms-and-conditions) on Wiley Online Library for rules of use; OA articles are governed by the applicable Creative Commons License

fabrication of pNIPAAm-based objects at the micrometer scale. More recently, polymerization triggered by multiphoton absorption has been demonstrated to provide a preparation technique for pNIPAAm-based microstructures with finer structural details.[17] In combination with metallic nanoparticles, the irradiated volume (where photoinitiation and polymerization occur) can be decreased to the nanoscale regime via the excitation of localized surface plasmon resonances in the near-infrared (NIR) part of the spectrum.[18]

Besides multiphoton initiation and polymerization of typically liquid monomers, an alternative approach can be employed for the fabrication of pNIPAAm structures by photocrosslinking of pre-synthesized polymer chains, which are solid in their dry state. This approach enables the preparation of structures from the compact dry polymer layer, without the risk of leaking the residual monomers when swollen, and benefits from facile means to incorporate multiple functionalities during the polymer pre-synthesis step. Additionally, the solid, uncrosslinked polymer layer can act as supporting material during the writing of complex 3D structures, which is a complicated task for the photopolymerization of liquid monomers that cannot support overhanging geometries (if not combined with, e.g., solid particle fillers [19]). In previous works, pNIPAAm-based biofunctional thin hydrogel films with polymer chains simultaneously crosslinked and attached to a gold surface upon irradiation with UV light were prepared with the use of self-assembled monolayer linkers carrying photoactive moieties.[20] The structuring of these layers was achieved by shadow mask lithography,[21] nanoimprint lithography,[22] or UV-laser interference lithography.[23,24] In these reports, pNIPAAm-based terpolymer with photocrosslinkable benzophenone groups and additional moieties for conjugating biomolecules[25] are used in bioanalytical applications as a tunable binding matrix for target analyte molecules.[26] Recently, this approach was further extended through the synthesis of polymers with even higher complexity and several incorporated functionalities in, e.g., thermoresponsive and thermochromic photocrosslinkable polymer systems.[27] Besides UV-triggered photocrosslinking, a multiphoton absorption process was also employed for the preparation of surface-attached 3D hydrogel structures from non-responsive (*N*,*N*-dimethyl acrylamide-based) and n-butylacrylate polymers.[28–30] In the context of biofunctional structures, the usage of an NIR beam for crosslinking of the hydrogel geometry provides the additional advantage of avoiding the risk of damaging delicate groups with UV light.

In the present work, we synthesized a new set of pNIPAAm-based co- and terpolymers bearing photoactive benzophenone and anthraquinone units for simultaneous multiphoton crosslinking and covalent attachment to a solid surface. To the best of our knowledge, this has not yet been demonstrated for this important thermoresponsive polymer and we investigate the efficiency of such fabrication route depending on the structural properties of prepared polymer scaffolds. An adaptable home-built lithographer with a femtosecond NIR laser was employed for structure writing after optimizing the photocrosslinking conditions. A series of optical and atomic force microscopy studies was implemented to reveal the structural and swelling properties of the prepared responsive hydrogel microstructures, as well as to evaluate the possibility of their post-modification with biomolecules.

2. Results and Discussion

As **Figure 1a** illustrates, the investigated polymers were deposited on a solid substrate in the form of a thin dry film for subsequent multiphoton writing of microstructures. Such writing was performed by scanning a focused femtosecond NIR laser beam at a wavelength of 785 nm to locally crosslink and anchor the polymer chains at the irradiated zones to the substrate. For this purpose, a series of pNIPAAm-based polymers was synthesized with a set of different photoactive groups, see Figure 1b. Benzophenone crosslinkers were incorporated into the pNIPAAm-based polymer chains by copolymerization of NIPAAm with *N*-(4-benzoylphenyl)acrylamide (BPAm) or [(4-benzoylphenyl)methyl]dimethyl[3-(prop-2-enamido)propyl]azanium bromide (BPQAAm). Anthraquinone side groups were integrated by copolymerization of NIPAAm with 2-acrylamido-3-hydroxyanthraquinone (AAHAQ) as well as 2-methacrylamido-3-hydroxyanthraquinone (MAAHAQ) monomers, respectively. Furthermore, a terpolymer of NIPAAm, BPQAAm, and methacrylic acid (MAA) was synthesized, bearing acid side groups for potential post-modification of the polymer networks enabling additional functionalities. The UV–vis absorption spectra of the corresponding crosslinker monomers in their most appropriate solvents and concentrations are presented in Figure 1c, illustrating their spectral differences.

2.1. Polymer Synthesis

For the synthesis of photocrosslinkable polymers, two fundamental strategies are applicable. In the first strategy, polymer molecules with reactive groups along the backbone can be conjugated in a post-polymerization modification with appropriate photocrosslinker units that carry the complementary reactivity. This conjugation approach has the advantage of modularity such that the same polymer system can be conjugated with different types of photocrosslinkers without affecting the degree of polymerization. Yet, an incomplete coupling reaction always results in a somewhat undefined polymer architecture and remaining reactive groups. In the second strategy, the main monomers

S. Fossati, J. Dostalek
FZU-Institute of Physics
Czech Academy of Sciences
Na Slovance 2, Prague 182 21, Czech Republic
N. G. Quilis
Biosensor Technologies
AIT-Austrian Institute of Technology
Konrad-Lorenz-Strasse 24, Tulln an der Donau 3430, Austria
C. Gusenbauer
Institute of Wood Technology and Renewable Materials
University of Natural Resources and Life Sciences
Konrad-Lorenz-Strasse 24, Tulln an der Donau 3430, Austria
B. Zbiral, J. L. Toca-Herrera
Institute of Biophysics
University of Natural Resources and Life Sciences
Muthgasse 11/II, Vienna 1190, Austria

© 2024 The Authors. Advanced Functional Materials published by Wiley-VCH GmbH

16163028, 2024, 26, Downloaded from https://onlinelibrary.wiley.com/doi/10.1002/adfm.202315578 by Readcube (Labtiva Inc.), Wiley Online Library on [01/07/2024]. See the Terms and Conditions (https://onlinelibrary.wiley.com/terms-and-conditions) on Wiley Online Library for rules of use; OA articles are governed by the applicable Creative Commons License

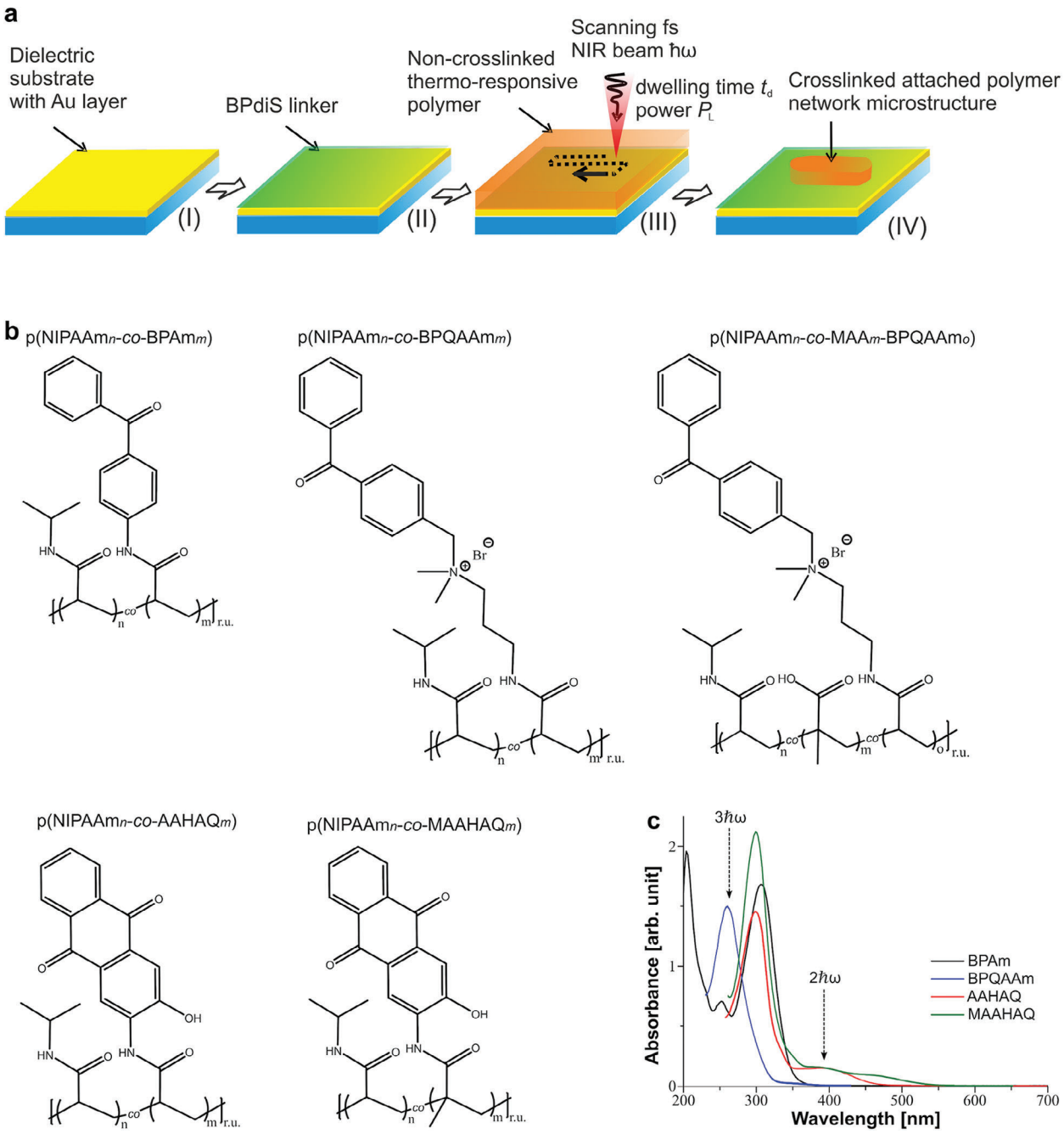

Figure 1. a) Schematic of the preparation of polymer network microstructures; b) chemical structures of the polymers and c) respective UV–vis spectra of the photoactive monomers (abbreviated as BPAm, BPQAAm, AAHAQ, and MAAHAQ according to the explanation in the main text) at the concentration of 0.048 g l^{-1} (in EtOH), 0.048 g l^{-1} (in water), 0.040 g l^{-1} (in DMSO), and 0.027 g l^{-1} (in DMSO), respectively after baseline correction for each solvent. The optimal absorption bands for two ($2\hbar\omega$) and three ($3\hbar\omega$) photon excitations are indicated in the spectra by arrows.

that determine the overall behavior of the polymer are copolymerized with comonomers that contain the photocrosslinkable units. This copolymerization approach requires a separate polymerization reaction for each type of photocrosslinker with an inherent slight variation of the resulting polymer structure (degree of polymerization, molar mass dispersity, and comonomer composition) between different samples. Nevertheless, very good control over the reaction conditions can be achieved to allow highly reproducible polymer architectures and the introduction of defined amounts of photocrosslinker units. Also, the combination of different types of comonomers in the same polymer backbone is achievable in this second approach. Thus, for the present paper, we have focused on this copolymerization strategy.

The literature-known BPAm crosslinker was synthesized by a variation of the published procedures.[20,31,32] Briefly,

© 2024 The Authors. Advanced Functional Materials published by Wiley-VCH GmbH

4-aminobenzophenone was exposed to an excess of acryloyl chloride, forming the BPAm monomer with a yield of 88%. The synthesis of BPQAAm was performed in a two-step reaction. In the first step, bromination by a Wohl-Ziegler-type reaction was performed according to the literature.[33] In short, 4-methylbenzophenone was brominated by *N*-bromosuccinimide via radical initiation with azobisisobutyronitrile (AIBN), yielding 84% of 4-bromomethyl benzophenone. In the second step, substitution of 4-bromomethyl benzophenone with *N*-[3-(dimethylamino)propyl]acrylamide in methyl *tert*-butyl ether led to precipitation of the final product BPQAAm as quaternary ammonium bromide in a yield of 90% (^{1}H and ^{13}C NMR spectra of the BPQAAm are shown in Figures S1 and S2, see SI). The anthraquinone-based crosslinker AAHAQ was prepared according to the literature by modification of 2-amino-3-hydroxyanthraquinone with an excess of acryloyl chloride in yields of up to 81%.[28] In an analogous reaction, the synthesis of the corresponding methacrylate MAAHAQ was attempted by treatment of 2-amino-3-hydroxyanthraquinone with a large excess of methacryloyl chloride. Yet, the ^{1}H NMR analysis of the isolated product (see Figure S3, Supporting Information) indicated incomplete conversion of the anthraquinone. Instead, a ratio of the product and the educt of MAAHAQ to 2-amino-3-hydroxyanthraquinone of 1:0.6 was found even after prolonged reaction times. Nevertheless, this product/educt combination was utilized in a polymerization reaction by adjusting the amount of the starting material mixture based on the above-mentioned ratio with the necessary monomer equivalents. This approach is legitimate, as the starting material without the methacrylic group is not incorporated into the chain during the polymerization reaction.

Copolymers containing the main monomer NIPAAm and one of the four different crosslinker monomers (BPAm, BPQAAm, AAHAQ, and MAAHAQ) were synthesized via free radical polymerization (see Scheme S1, Supporting Information). Specific details about the copolymerization procedures and the copolymer composition can be found in the Figures S4–S16 (Supporting Information).

Overall, the copolymerization of NIPAAm with BPAm or BPQAAm at crosslinker feeds of 1% and 5% resulted in reasonable yields of 60%–80%. As expected from a free radical mechanism, high apparent molar masses (75–150 kDa) and broad molar distributions ($Đ$ = 2.39-2.97) were attained, as determined by size-exclusion chromatography (SEC, see Figure S4, Supporting Information). In contrast, the yields of 22%–51% for the AAHAQ-containing copolymers were significantly lower, the apparent molar masses only amounted to 23–30 kDa, and the molar mass curves from SEC showed a surprisingly narrow and symmetric shape reminiscent of a Poisson distribution (see Figure S5, Supporting Information). It is very striking that nearly all copolymers with AAHAQ prepared by free radical polymerization exhibit narrow dispersities of $Đ$ = 1.3–1.5. Values close to $Đ$ = 1 are typically found for living or controlled radical chain growth mechanisms, such as radical addition-fragmentation chain transfer (RAFT) polymerization.[34,35] Under the assumption that only termination by combination prevails, the theoretical lower limit of the molar mass distribution for free radical polymerization is $Đ$ = 1.5.[36] Thus, the here observed low dispersities for the AAHAQ-containing copolymers suggest a chain transfer reaction mediated by the anthraquinone monomer. A narrow dispersity of $Đ$ = 1.8, which is unusual for free radical polymerizations, was reported in the literature for copolymers composed of AAHAQ and methyl methacrylate,[37] supporting the assumption of the anthraquinone group being involved in the chain growth mechanism. For the MAAHAQ-containing copolymers, the yields of 30%–68% are somewhat higher compared to copolymers with AAHAQ, while they still possess similar apparent molar masses in the range of 27.8–36.9 kDa and narrow dispersities of $Đ$ = 1.3–1.6 (see Figure S6, Supporting Information). As for the copolymerization with AAHAQ, the experimental results indicate an involvement of the MAHAAQ in the chain growth mechanism. However, the postulated transfer mechanism including the anthraquinone crosslinker monomers appears to be complex and was not systematically investigated at this point. This question will be a topic for future studies.

For potential post-modification, 5 mol% methacrylic acid (MAA) was included in the NIPAAm-based terpolymer containing 1 mol% BPQAAm (see Scheme S2, Supporting Information). The carboxylic acid functions of the MAA groups allow the subsequent introduction of molecular fragments (such as biological ligands like antibodies) into the polymer networks after photocrosslinking. The yield of 73% for the terpolymer was comparable to that of the copolymer solely from NIPAAm and BPQAAm, with a similar apparent molar mass of 97 kDa and a dispersity of $Đ$ = 1.89 (see Figure S7, Supporting Information). Furthermore, terpolymers could be prepared from NIPAAm with feeds of 5 mol% MAA and 1 mol% of the two anthraquinone crosslinker monomers, respectively (see Supporting Information).

UV–vis absorption spectra of the used photoactive monomers are shown in Figure 1c and reveal that the spectral position of their absorption peaks varies depending on the crosslinker and the way it is conjugated with the polymer backbone. The BPQAAm monomer exhibits an absorption spectrum with a single peak centered at a wavelength of ≈260 nm, which is close to the energy corresponding to the three-photon absorption process (wavelength of 261 nm) with an NIR light beam at a wavelength of 785 nm. All other crosslinkers show a red-shifted absorption peak located at wavelengths 300–325 nm, which is in the spectral range between a three-photon absorption process (wavelength of 261 nm) and a two-photon absorption process (wavelength of 392 nm). However, AAHAQ and MAAHAQ monomers show an additional shoulder of the absorption peak overlapping with the wavelength of 392 nm making them potentially suitable for a two-photon absorption process. Similar UV–vis absorption bands were observed for the synthesized copolymers (see Figures S12–S15, Supporting Information).

2.2. Multiphoton Photochemical Crosslinking of the Polymer Networks

In order to anchor the polymer chains to a gold layer deposited on a BK7 glass substrate, the gold surface was first reacted with 3,3′-disulfanediylbis(N-(4-benzoylbenzyl)propanamide, in short benzophenone disulfide (BPdiS) linker.[38] BPdiS allowed the formation of a self-assembled monolayer (SAM) before the deposition of investigated polymers that were spun on the surface to yield a layer with a thickness of ≈100 nm (as determined by

© 2024 The Authors. Advanced Functional Materials published by Wiley-VCH GmbH

16163028, 2024, 26, Downloaded from https://onlinelibrary.wiley.com/doi/10.1002/adfm.202315578 by Readcube (Labtiva Inc.), Wiley Online Library on [01/07/2024]. See the Terms and Conditions (https://onlinelibrary.wiley.com/terms-and-conditions) on Wiley Online Library for rules of use; OA articles are governed by the applicable Creative Commons License

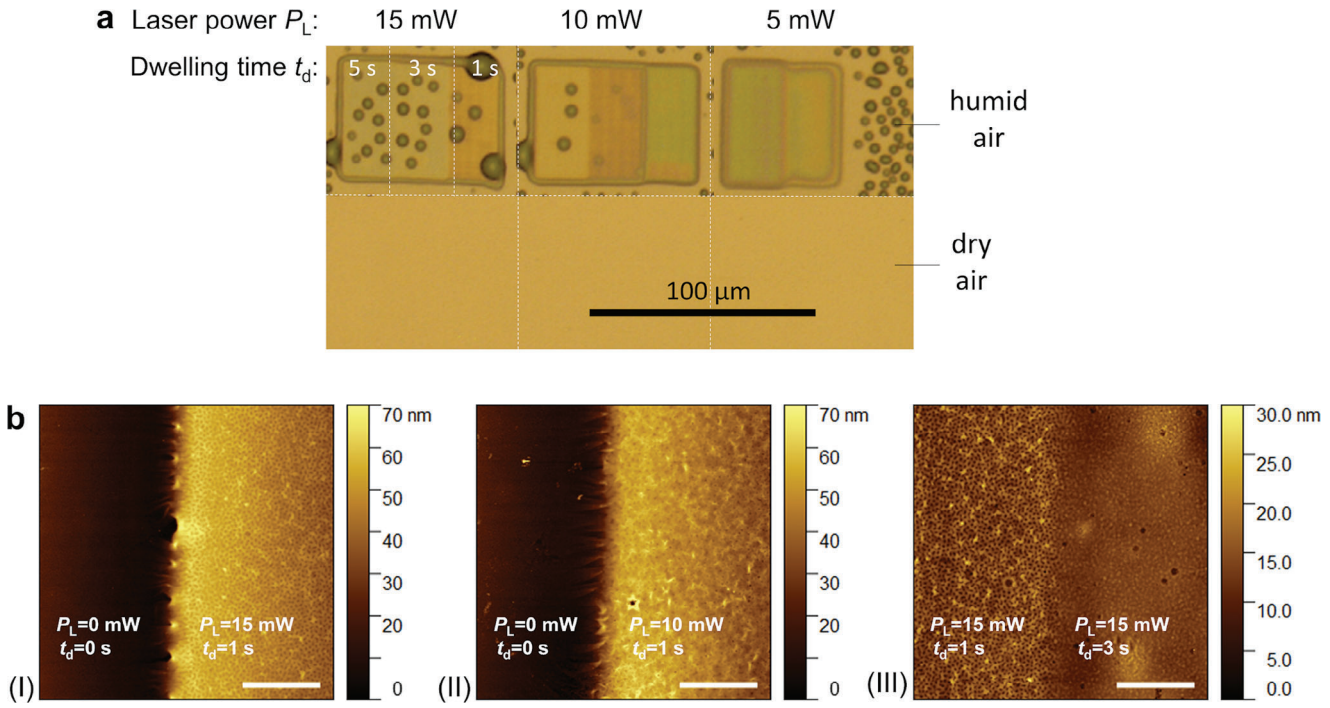

Figure 2. a) Bright-field optical microscopy images structures prepared from poly(NIPAAm$_{95}$-*co*-BPQAAm$_5$) with indicated combinations of P_L and t_d when exposed to dry air (bottom row) and humid air in order to form a hydrogel (upper row). b) AFM images of the same poly(NIPAAm$_{95}$-*co*-BPQAAm$_5$) structures on the border of the bare gold substrate and the polymer layer prepared with i) P_L of 15 mW and t_d of 1 s; ii) P_L of 10 mW and t_d of 1 s; and iii) between two polymer network regions made with P_L of 15 mW, t_d of 1 s and P_L of 15 mW, t_d of 3 s; the scale bar is 5 µm.

surface plasmon resonance after drying, see Figure S17, Supporting Information). These substrates were then mounted to a home-built multiphoton lithographer (for more detail see Figure S18, Supporting Information and the Experimental section) that was equipped with a laser emitting ≈100 fs pulses at a repetition rate of 80 MHz. This laser beam was focused through the air on the polymer layer by a 40× objective and the irradiated spot diameter was estimated to be <5 µm (for the given NIR laser beam divergence). The effective power P_L of the beam focused on the polymer sample was controlled between 5 and 15 mW and the overall dose received by the sample at the focal spot was defined by the dwelling time t_d set between 1 and 5 s. The focused beam was raster scanned over the sample by using a motorized stage with a movement step of 1 µm.

To test the ability of the polymer samples to form a hydrogel layer via crosslinking by a multiphoton absorption process, a series of rectangular pads with the size of 75×50 µm^2 were recorded in the polymer layers for nine combinations of dwelling time t_d and irradiation power P_L for each polymer type. After the recording, uncrosslinked polymer chains in non-irradiated areas were dissolved by rinsing the substrate with ethanol, eventually leaving only the irradiated pads with successfully crosslinked and attached polymer chains.

First, the presence of the pads in contact with dry and humid air was optically examined by bright-field optical microscopy. The prepared pads were not visible in the dry state, however, water molecules diffused into the polymer network upon exposure to humid air causing their swelling, and then the increased optical contrast allowed for clear observation of their structure. These structures were examined for all synthesized polymers (see Figure S19, Supporting Information) and an example is provided in **Figure 2a** for the poly(NIPAAm$_{95}$-*co*-BPQAAm$_5$). For irradiation laser power set to P_L = 5 mW, the threshold dwelling time t_d that resulted in a stable poly(NIPAAm$_{95}$-*co*-BPQAAm$_5$) network was found to lie above 1 s. For lower irradiation doses no crosslinking took place and the polymer in the irradiated regions did dissolve. When increasing the irradiation power to P_L = 10 and 15 mW, the threshold dwelling time decreased below 1 s. When decreasing the amount of photocrosslinker content in the polymer chains from 5% to 1%, the threshold dwelling time also increased, as can be seen in Figure S20 (Supporting Information) for the poly(NIPAAm$_{99}$-*co*-BPQAAm$_1$). Afterward, the topography of dry samples was examined with atomic force microscopy (AFM), as presented in Figure 2b (AFM images with the corresponding height cross-sections can be found in Figure S21, Supporting Information). The image of the structure edge shows a height of ≈50–60 nm, which is lower than the thickness of the polymer layer before the recording and indicates that a fraction of unbound polymer chains was extracted from the network structures upon rinsing.

Moreover, one can notice a smearing of the structure at the edges, which can be attributed to the effect of swelling. In addition, the stronger crosslinked pads (irradiated with P_L = 15 mW and t_d = 1 s) show a characteristic pore structure resembling wrinkle-patterned hydrogels.[39–41] Besides being of fundamental interest, wrinkle-pattern engineering of the hydrogels offers promising design principles for future smart systems.[42,43]

Interestingly, the polymer poly(NIPAAm$_{95}$-*co*-BPQAAm$_5$) with benzophenone crosslinker BPQAAm (containing a

© 2024 The Authors. Advanced Functional Materials published by Wiley-VCH GmbH

16163028, 2024, 26, Downloaded from https://onlinelibrary.wiley.com/doi/10.1002/adfm.202315578 by Readcube (Labtiva Inc.), Wiley Online Library on [01/07/2024]. See the Terms and Conditions (https://onlinelibrary.wiley.com/terms-and-conditions) on Wiley Online Library for rules of use; OA articles are governed by the applicable Creative Commons License

16163028, 2024, 26, Downloaded from https://onlinelibrary.wiley.com/doi/10.1002/adfm.202315578 by Readcube (Labtiva Inc.), Wiley Online Library on [01/07/2024]. See the Terms and Conditions (https://onlinelibrary.wiley.com/terms-and-conditions) on Wiley Online Library for rules of use; OA articles are governed by the applicable Creative Commons License

quaternary ammonium fragment) was the only NIPAAm-based polymer that allowed a reliable preparation of thin hydrogel microstructures via the multiphoton absorption crosslinking process. For the other polymer poly(NIPAAm$_{95}$-*co*-BPAm$_5$) with the benzophenone acrylamide crosslinker BPAm (conjugated to the polymer backbone without the ammonium group), we observed that the same illumination conditions did not yield a hydrophilic network and the obtained structures showed a more hydrophobic character that may be ascribed to pyrolysis of the polymer (see Figure S19, Supporting Information). This hypothesis is supported by AFM measurements of the irradiated poly(NIPAAm$_{95}$-*co*-BPAm$_5$) film, which is characterized by inhomogeneous and rather irregular structures (Figure S22, Supporting Information). The difference between the poly(NIPAAm$_{95}$-*co*-BPAm$_5$) and poly(NIPAAm$_{95}$-*co*-BPQAAm$_5$) microstructures is even more obvious when comparing AFM peak force amplitude maps (Figure S23, Supporting Information), where the poly(NIPAAm$_{95}$-*co*-BPAm$_5$) microstructures are reminiscent of a material edge after the laser ablation.[44] The experimentally accessible irradiation conditions for the photocrosslinking of NIPAAm-based polymers with anthraquinone groups – poly(NIPAAm$_{95}$-*co*-AAHAQ$_5$) and poly(NIPAAm$_{95}$-*co*-MAAHAQ$_5$) – apparently did not lead to network formation, as the layers were washed away for all tested dwelling times t_d and irradiation power values P_L (see Figure S19, Supporting Information). On the other hand, a single-photon crosslinking process with 5 mol% AAHAQ crosslinker content in the pNIPAAm polymer at 254 nm irradiation wavelength, starting with a dose of 8.6 J cm^{-2}, induced crosslinking and formation of a stable hydrogel after swelling with water (see Figures S25, S26 and Tables S4, S5, Supporting Information). When irradiating at a longer wavelength of 365 nm, an irradiation dose above 10 J cm^{-2} was required to achieve crosslinking. Also, when employing pNIPAAm polymers with only 1 mol% AAHAQ crosslinker content, no network formation was observed under the above irradiation conditions. Similar as reported in the literature,[28,29] the multiphoton-absorption crosslinking led to the formation of polymer networks when using the same AAHAQ crosslinker but exchanging the main monomer with *N*,*N*-dimethyl acrylamide (DMAA) to yield the polymer poly(DMAA$_{95}$-*co*-AAHAQ$_5$) (see Scheme S3, Figure S20, bottom row, and Figure S27, Supporting Information).

These findings are to be explained by the structural differences of the polymer scaffolds upon variation of the main monomer and the photocrosslinker chromophore, substantially affecting the excitation mechanism of multiphoton-absorption and the crosslinking reaction cascade. Considering first the main monomers, DMAA is a tertiary amide that bears two methyl groups directly bound to the nitrogen atom, while NIPAAm is a secondary amide possessing one hydrogen atom directly attached to the nitrogen (engaging in hydrogen bonding interactions) and one labile hydrogen at the tertiary carbon of the *iso*-propyl group. The latter hydrogen atom at the tertiary carbon is susceptible to radical abstraction by homolytic cleavage, resulting in a carbon radical that is stabilized by hyperconjugation with the tertiary framework. While the NIPAAm-based polymer is indeed able to undergo crosslinking in the *single* photon absorption process for both the AAHAQ-based as well as for benzophenone-based crosslinker comonomers,[20,32,45,46] the *multi*photon crosslinking

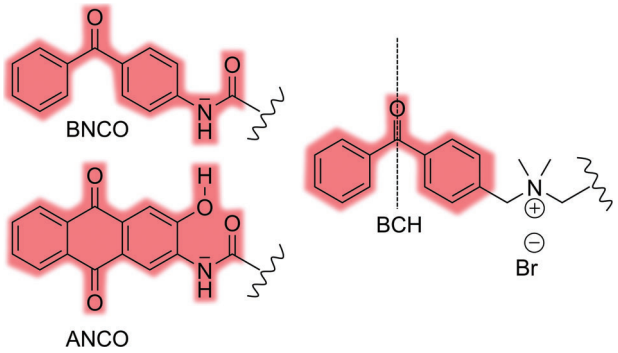

Figure 3. Schematics of the three distinct shapes BNCO, BCH, and ANCO for the respective crosslinker chromophores of BPAm, BPQAAm, as well as AAHAQ and MAAHAQ, with the electronically coupled conjugated regions highlighted in red. The black dotted line in BCH indicates the orbital mirror symmetry plane.

was only successful with the BPQAAm unit. Thus, considering only the effects of the main monomer is not sufficient to explain the observed phenomena. In an attempt to elucidate the *multi*photon mechanism, the characteristics of the crosslinker chromophores also need to be scrutinized. In **Figure 3**, the different extensions of the electronic systems are visualized in the four crosslinker monomers employed in the present study. In these schematics, the three distinct shapes of the conjugated regions are abbreviated as BNCO for BPAm, BCH for BPQAAm, and ANCO for both AAHAQ and MAAHAQ. The variation in multiphoton excitation upon irradiation is attributed to the different shapes of these electronic structures, specifically a difference in symmetry, with BCH having a mirror symmetry plane cutting through the carbonyl bond (Figure 3, black dotted line) to support odd-number multiphoton absorption processes (like $3\hbar\omega$). Such mirror plane is missing from BNCO and ANCO, thus they would allow even-number multiphoton absorption processes (like $2\hbar\omega$).

The chromophores BNCO and ANCO exhibit extended conjugated systems involving the amide groups, whereas the conjugation path of BCH only spans over the carbonyl group and the two aromatic rings. The presence of the amide group apparently hampers the multiphoton-induced crosslinking reaction. For BCH a different reaction scenario upon multiphoton excitation can be envisioned, which is displayed in **Figure 4**. The assumed reaction cascade starts with a classical photoexcitation of the carbonyl group in I, where the biradical II is formed at the benzophenone ketone group, as stated in various references of the literature.[46–49] The radical site on the oxygen atom of this carbonyl biradical can abstract a hydrogen atom from a polymer chain in its proximity, resulting in a hydroxyl group on the carbonyl carbon radical and leaving a carbon-based radical site on the participating neighboring polymer chain (III). Following the common mechanism from literature for single-photon crosslinking mentioned above, the carbon radical center of the carbonyl group combines with the carbon-based radical of the adjacent polymer chain, forming a crosslink (see Figure 4, "direct crosslinking (1)" pathway, X).

An alternative reaction pathway for the multiphoton excitation of BCH follows a mesomeric dislocation of the single electron from the carbon-based radical in III via IV to the 4-position in the

© 2024 The Authors. Advanced Functional Materials published by Wiley-VCH GmbH

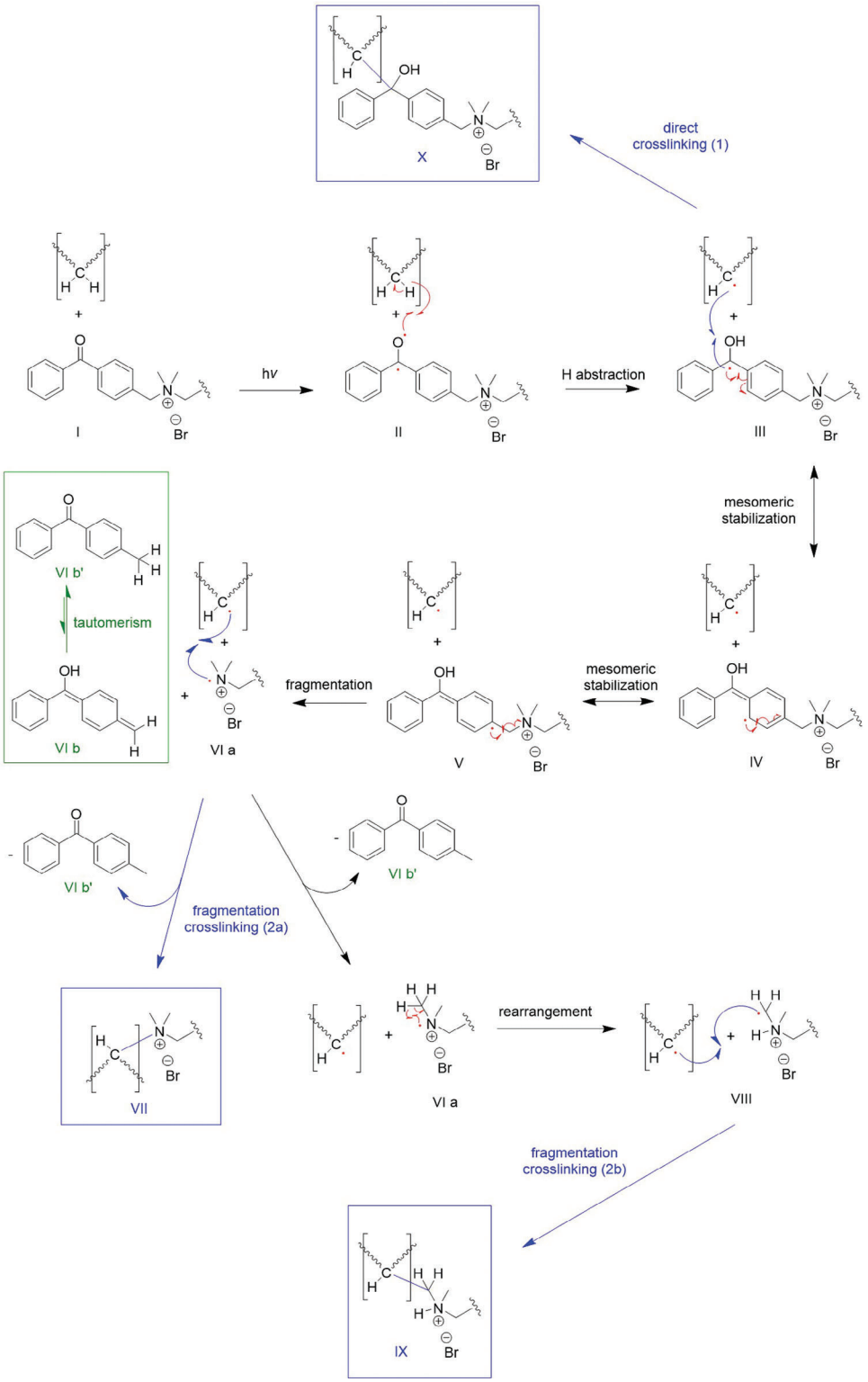

Figure 4. The hypothetical mechanism for the multiphoton absorption crosslinking process [fragmentation crosslinking (2a) and fragmentation crosslinking (2b)] of BPQAAm compared with the direct crosslinking mechanism [direct crosslinking (1)]. Square brackets are only schematic indications for a generic polymer chain structure and are not intended to represent the exact repeat unit.

© 2024 The Authors. Advanced Functional Materials published by Wiley-VCH GmbH

16163028, 2024, 26, Downloaded from https://onlinelibrary.wiley.com/doi/10.1002/adfm.202315578 by Readcube (Labtiva Inc.), Wiley Online Library on [01/07/2024]. See the Terms and Conditions (https://onlinelibrary.wiley.com/terms-and-conditions) on Wiley Online Library for rules of use; OA articles are governed by the applicable Creative Commons License

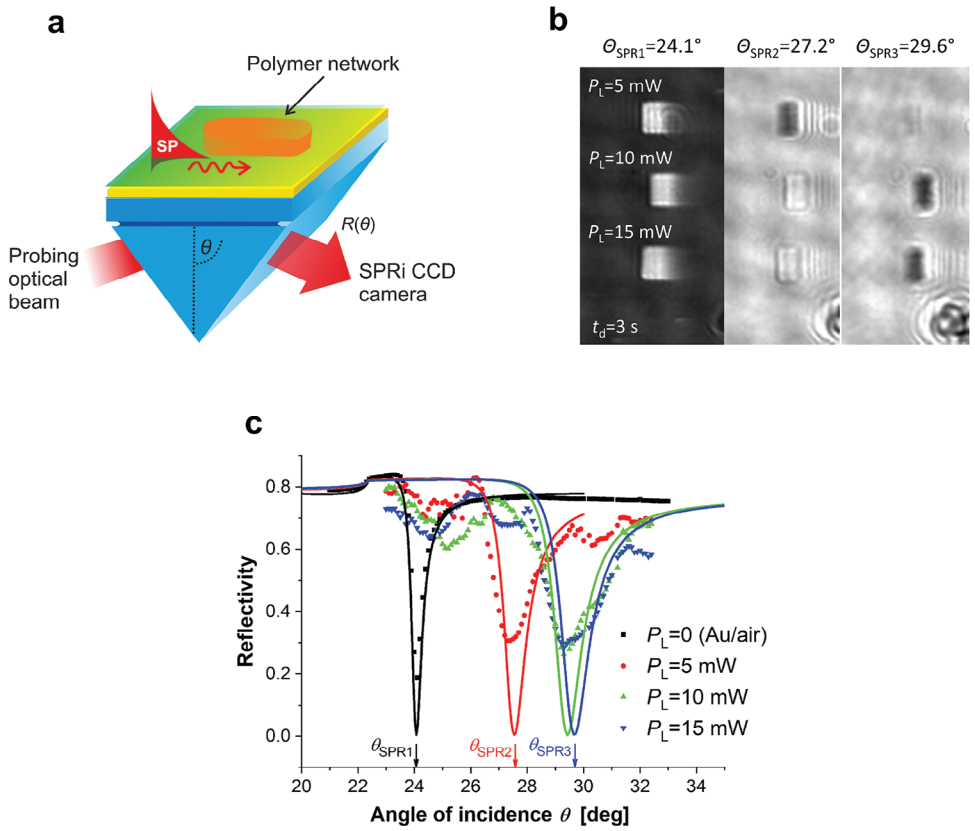

Figure 5. a) Schematics of the SPRi setup employed for probing the pNIPAAm-based microstructures in the air; b) SPRi images and c) corresponding angular reflectivity spectra in the air for the case of poly(NIPAAm$_{95}$-*co*-BPQAAm$_5$) structures made with a constant dwelling time of t_d = 3 s and varying the laser power P_L between 5, 10, or 15 mW. Solid curves in Figure 5c represent fits calculated with the Fresnel-based reflectivity model.

benzophenone unit (V), where the methylene bridge is attached to a quaternary ammonium group. At this point, a homolytic cleavage of the sigma bond between the methylene carbon and the nitrogen atom from the quaternary ammonium group may take place, resulting in the quinoid form VI b of benzophenone and the fragment VI a with a radical cation on the nitrogen atom. This hypothesis is supported by literature reports on the formation of such nitrogen-based radical cations.[50] This N-radical cation could undergo a crosslinking reaction with an adjacent polymer chain (see Figure 4, "fragmentation crosslinking (2a)" pathway, VII), and forming 4-methylbenzophenone VI b' as the byproduct of the reaction after tautomeric rearrangement of the quinoid benzophenone form VI b.[51]

Yet, an additional reaction pathway may involve a hydrogen shift from the methyl group of the ammonium moiety to the nitrogen radical cation VI a. The formed methylene radical VIII can undergo crosslinking by combination with the polymer backbone radical (see Figure 4, "fragmentation crosslinking (2b)" pathway, IX), also leading to 4-methylbenzophenone (VI b') as a side product.

At this point, we do not have the means of detailed chemical characterization of the crosslinking products of the thin hydrogel films to verify these reaction pathways, but on the basis of existing literature, the drawn assumptions are highly plausible. Nevertheless, the experimental results clearly indicate successful multiphoton crosslinking for the BPQAAm-containing polymers, and further investigation is needed to reveal the underlying photocrosslinking mechanism.

In order to characterize the swelling properties of the prepared hydrogel microstructures, the surface plasmon resonance imaging (SPRi) technique was exploited (**Figure** 5a). A glass substrate was coated with a 50 nm gold film, equipped with a SAM of BPdiS, thin films of the pNIPAAm-based polymers were deposited. After drying, the layers were locally crosslinked and surface-attached by irradiation with a focused laser. The thickness of the prepared pNIPAAm-based polymers layers was adjusted to ≈50 nm (in the dry state as showed by the previous AFM study, see Figure 2) in order to match it with the probing depth of surface plasmon waves (typically reaching 100 nm for used optical parameters). The surface of this substrate was probed by an expanded monochromatic beam that was resonantly coupled to surface plasmon waves traveling along the outer gold interface (for more details about the home-built SPRi setup refer to Figure S28, Supporting Information and the Experimental section). For the resonant excitation of surface plasmon waves, the attenuated total internal reflection method with Kretschmann geometry was used by optically matching the glass substrate to a prism. The spatial distribution of the reflected light intensity was measured by a CCD camera to interrogate changes in surface plasmon resonance (SPR) occurring due to the variations in thermoresponsive hydrogel layers. It manifests itself as a decrease in the reflected intensity that can be tuned by changing the angle

© 2024 The Authors. Advanced Functional Materials published by Wiley-VCH GmbH

16163028, 2024, 26, Downloaded from https://onlinelibrary.wiley.com/doi/10.1002/adfm.202315578 by Readcube (Labtiva Inc.), Wiley Online Library on [01/07/2024]. See the Terms and Conditions (https://onlinelibrary.wiley.com/terms-and-conditions) on Wiley Online Library for rules of use; OA articles are governed by the applicable Creative Commons License

16163028, 2024, 26, Downloaded from https://onlinelibrary.wiley.com/doi/10.1002/adfm.202315578 by Readcube (Labtiva Inc.), Wiley Online Library on [01/07/2024]. See the Terms and Conditions (https://onlinelibrary.wiley.com/terms-and-conditions) on Wiley Online Library for rules of use; OA articles are governed by the applicable Creative Commons License

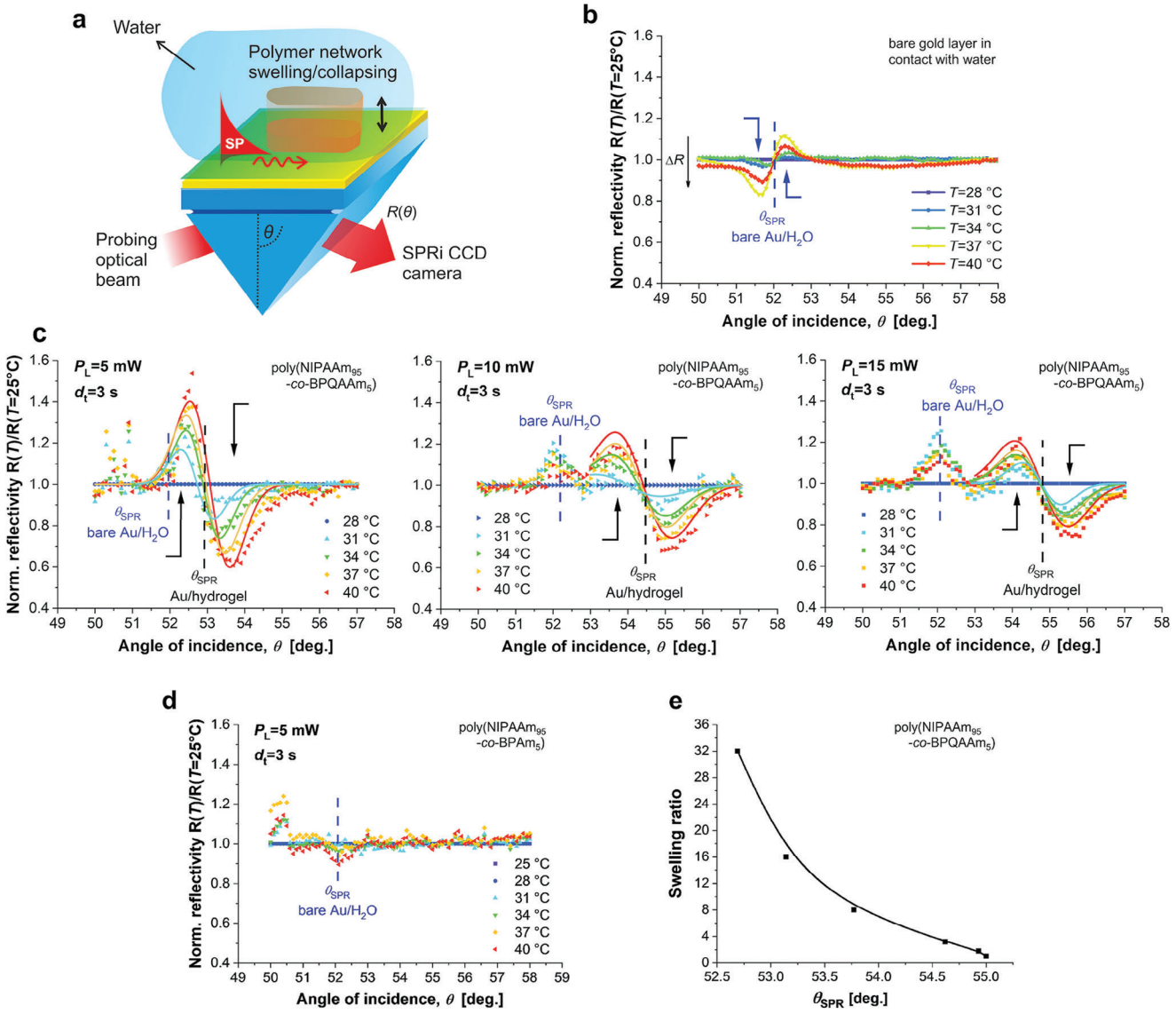

Figure 6. a) Schematics of the SPRi employed for probing the pNIPAAm-based microstructures in water. Normalized angular reflectivity spectra in milliQ water with respect to the water temperature for b) the bare gold layer, c) poly(NIPAAm$_{95}$-*co*-BPQAAm$_5$) crosslinked structures at P_L of 5, 10, or 15 mW and t_d = 3 s and d) poly(NIPAAm$_{95}$-*co*-BPAm$_5$) crosslinked structure at P_L of 5 mW and t_d = 3 s; e) dependence between the hydrogel swelling ratio and the SPR angle for the case of the poly(NIPAAm$_{95}$-*co*-BPQAAm$_5$) hydrogel.

of incidence (see Figure 5b). The minimum reflectivity occurs at the resonance angle θ_{SPR} where surface plasmon waves are excited with the highest efficiency through the resonant optical coupling. From a series of SPRi images acquired at varied angles of incidence, angular reflectivity curves were established for the examined distinct areas carrying the crosslinked pNIPAAm-based microstructures. In this experiment, the dwelling time was set to t_d = 3 s and the laser power P_L varied from 15, 10, to 5 mW to write the polymer network structures, defining three spatially separated pads. The obtained data presented in Figure 5c were acquired for dry polymer pads and were fitted for each crosslinking condition with a model based on the Fresnel multilayer reflectivity formalism to determine the layer thickness. Given a refractive index (RI) for pNIPAAm of 1.49 at λ = 785 nm,[52] the fitted thickness for the dry polymer pads prepared with P_L = 5, 10, and 15 mW amounted to 30.5, 41.2, and 42.5 nm, respectively. These thickness values are in good agreement with the data obtained by AFM measurements (compare Figure S21, Supporting Information).

It should be noted that the acquired angular reflectivity spectra show artifacts that are ascribed to interference effects between the surface plasmon waves excited at the bare gold surface and traveling through the pNIPAAm-based structures with those resonantly excited in the polymer-coated areas and due to reflecting of these waves at interfaces. Therefore, for the investigation of the temperature-dependent swelling when in contact with water (**Figure 6a**), the reflectivity curves were measured for increasing temperature T from 28 to 40 °C and normalized with the dependence measured at T = 25 °C. Figure 6b presents such processed reflectivity curves for the bare gold surface in contact with water

© 2024 The Authors. Advanced Functional Materials published by Wiley-VCH GmbH

that serves as a reference. One can see that increasing temperature leads to the occurrence of a feature with an inflection point centered at the angle of incidence corresponding to $\theta_{SPR} = 52°$. This feature exhibits a lower signal at angles $< \theta_{SPR}$ and a higher signal at angles $> \theta_{SPR}$ (which is indicated by blue bent arrows), and it apparently corresponds to the effect of decreasing the SPR angle θ_{SPR} due to increasing temperature. This agrees with the optical properties of water refractive index which drops when increasing temperature T.[53]

When analyzing the normalized curves measured on the areas coated with hydrogel prepared from poly(NIPAAm$_{95}$-*co*-BPQAAm$_5$), a similar feature with the inflection point can be seen at θ_{SPR} that is shifted to higher angles (see Figure 6c). The reason for this shift is the higher refractive index of the hydrogel with respect to that of water. Importantly, the temperature-induced changes in the vicinity of the inflection point are opposite to that for bare gold, i.e., when increasing the temperature, the signal increases at angles $< \theta_{SPR}$ and decreases at $> \theta_{SPR}$ (which is indicated by black bent arrows). This is a clear signature that the refractive index of pNIPAAm-based networks increases with temperature T upon its collapse. As can be seen in Figure 6c, this effect occurs at temperatures > 31 °C where pNIPAAm has its LCST. For comparison, we included data in Figure 6d measured for poly(NIPAAm$_{95}$-*co*-BPAm$_5$), which does not show a significant response to the temperature changes. This evidence supports the hypothesis that the polymer network was not formed from the polymer with BPAm crosslinker and that no hydrogel structures were formed, e.g., due to pyrolysis of the polymer.

After proving that the pNIPAAm-based hydrogel microstructures prepared by crosslinking with the multiphoton absorption process retain thermoresponsive characteristics, their swelling ratio was deduced from the SPRi analysis. By using a Fresnel-based theory, we established a dependence of the swelling ratio on the SPR angle θ_{SPR} for the prepared films assuming that the surface mass density is preserved upon the swelling and collapsing and that in the fully collapsed state, the thickness and refractive index of the hydrogel is the same as that determined for the dry films. By comparing the measured $\theta_{SPR} = 53°$ of the weakly crosslinked hydrogel ($t_d = 3$ s, $P_L = 5$ mW) with that determined for the dry film, it can be estimated that the swelling ratio exceeds a factor of 10 (Figure 6e). This quantity refers to the ratio of thickness in the swollen and dry state and the obtained value is higher than that of similar pNIPAAm-based hydrogel films previously prepared by one-photon absorption with the use of UV photocrosslinking.[20,21]

2.3. Responsivity and Post-Modification of the Polymer Network with Biomolecules

Besides the binary copolymer of NIPAAm and BPQAAm, a terpolymer with additional MAA units was investigated in order to enable the post-modification of prepared polymer networks. For that purpose, the polymer poly(NIPAAm$_{94}$-*co*-MAA$_5$-BPQAAm$_1$) was synthesized and used for surface-attached microstructures prepared by multiphoton photocrosslinking. Similar terpolymers were also synthesized with the two anthraquinone crosslinkers AAHAQ and MAAHAQ, but no crosslinking with multiphoton irradiation could be achieved in these cases, as observed before with the corresponding copolymers. The swelling and thermoresponsive properties of poly(NIPAAm$_{94}$-*co*-MAA$_5$-BPQAAm$_1$) were examined by AFM operated in contact mode in a liquid medium (milliQ water) kept at a fixed temperature. These measurements were carried out to determine the temperature-dependent mechanical stability of the network as presented in **Figure 7**. The data show that for the hydrogels prepared with $t_d = 3$ s and 5 s and irradiation power P_L of 10 mW, Young's modulus increased from 19 to 26 kPa and from 26 to 30 kPa (respectively) when increasing the temperature from 25 to 40 °C. This documents a collapse of the prepared hydrogel microstructures at temperatures above the pNIPAAm's LCST, yielding a denser and stiffer polymer network.

As this terpolymer bears carboxyl MAA groups, it can be modified with biomolecules through established amine coupling chemistry.[20,54,55] This possibility was demonstrated on a gold-coated substrate with two hydrogel pads fabricated with the $t_d = 3$ s and $P_L = 15$ mW. After recording the structure and developing it by rinsing with ethanol to remove the non-crosslinked polymer chains, the MAA groups were activated by active ester chemistry. Then, IgG protein molecules labeled with Alexa Fluor 647 dye were covalently coupled to the network via their amine groups. The presence of the polymer pads is documented in the bright-field microscopy image, **Figure 8a**. The position of these pads aligns well with the bright areas observed with a confocal fluorescence microscope after the coupling of IgG molecules, Figure 8b. These measurements were performed when the structures were swollen in water, which allowed to increase distance between the metal surface and fluorophores tagged to IgG molecules and thus to reduce quenching. The inset shows an image of one of the pads taken with increased magnification and it interestingly exhibits apparent darker areas resembling the pores observed by AFM for similar hydrogel films (see Figure S21, Supporting Information). It is worth noting that the fluorescence signal originates from anchored IgG molecules tagged with Alexa Fluor 647 . Our previous studies, where a similar pNIPAAm polymer network was used as an affinity binding matrix, showed negligible autofluorescence of the bare structure for the same excitation and emission wavelengths.[21,24]

3. Conclusion

This work demonstrates multiphoton absorption–based crosslinking of polymer chains for the facile preparation of thermoresponsive biofunctional NIPAAm-based hydrogel microstructures. A set of NIPAAm-based copolymers and terpolymers was synthesized with controlled amounts of anthraquinone or benzophenone photocrosslinkers conjugated by different structural spacers to the polymer backbone. The study revealed that the ability to crosslink the polymers not only depends on the parameters of the NIR pulsed laser beam scanned over the sample, but also on the choice of the photocrosslinking unit, the spacer between the photocrosslinker and polymer chains, and the nature of the polymer backbone. The results show that for AAHAQ and MAAHAQ crosslinkers attached to the pNIPAAm polymer backbone, the experimentally accessible irradiation dose did not allow reaching the crosslinking

© 2024 The Authors. Advanced Functional Materials published by Wiley-VCH GmbH

16163028, 2024, 26, Downloaded from https://onlinelibrary.wiley.com/doi/10.1002/adfm.202315578 by Readcube (Labtiva Inc.), Wiley Online Library on [01/07/2024]. See the Terms and Conditions (https://onlinelibrary.wiley.com/terms-and-conditions) on Wiley Online Library for rules of use; OA articles are governed by the applicable Creative Commons License

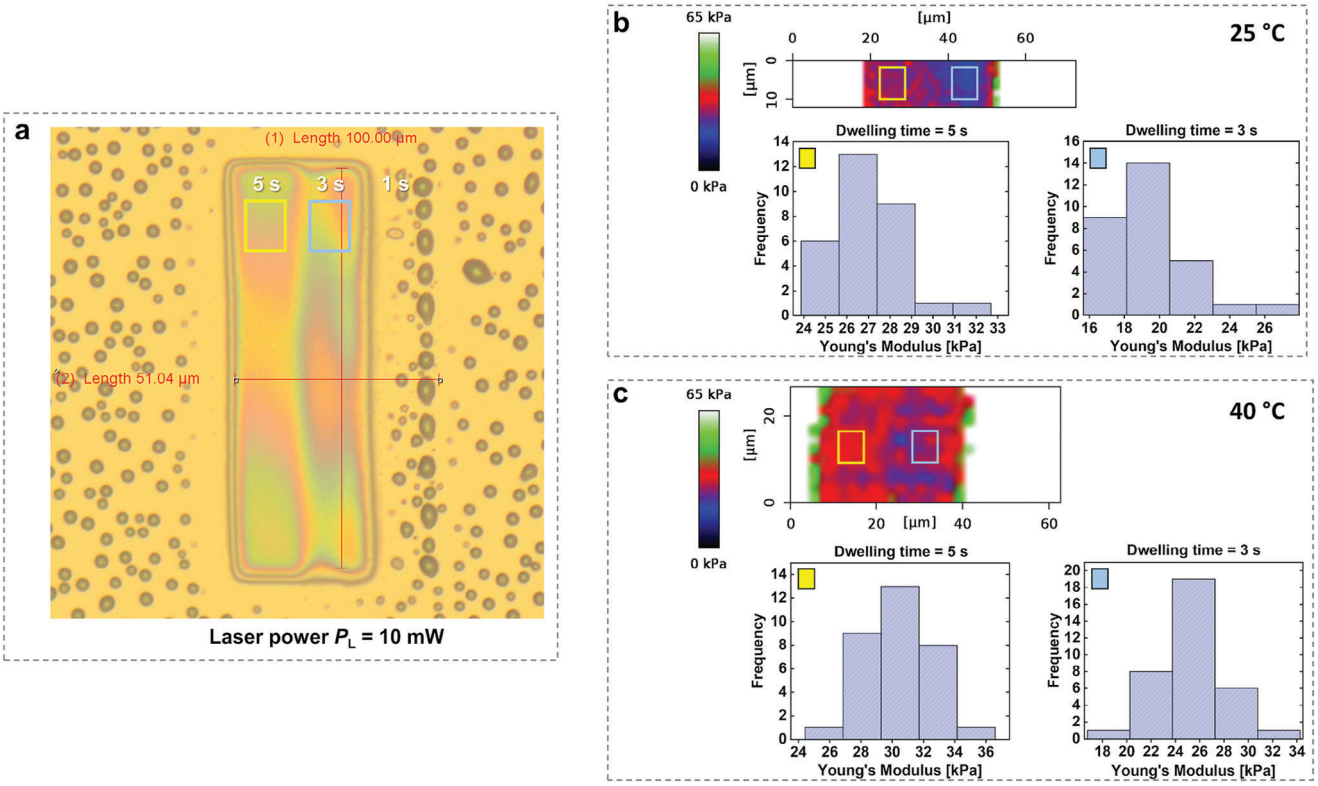

Figure 7. Temperature-controlled AFM measurements of Young's moduli for a poly(NIPAAm$_{94}$-*co*-MAA$_5$-BPQAAm$_1$) hydrogel pad made with a laser power P_L of 10 mW and dwelling times t_d of 1, 3, and 5 s on a BK7 substrate. a) Bright-field microscopy image of the formed hydrogels and water condensation patterns after exposure to humid air. Histograms of measured Young's moduli at b) 25 °C and c) 40 °C. Blue and yellow rectangles mark the regions where the modulus distributions were measured.

threshold (however, when changing the polymer backbone to DMAA, successful network preparation was possible). The combination of the BPAm crosslinker with the pNIPAAm polymer backbone assumably showed the effect of pyrolysis and only the BPQAAm crosslinker allowed to yield robust, spatial controllable protocol for the preparation of the pNIPAAm-based polymer networks. The hypothetical pathways for crosslinking mechanism in the case of BPQAAm-based polymer were proposed and discussed; however, a furthermore comprehensive study is needed to confirm the hypothesis. For the identification of the best-performing poly(NIPAAm-*co*-BPQAAm) polymer, the dependence of the threshold on the photocrosslinker amount was determined for different irradiation intensities and dwelling times of the NIR laser beam. Interestingly, the formation of

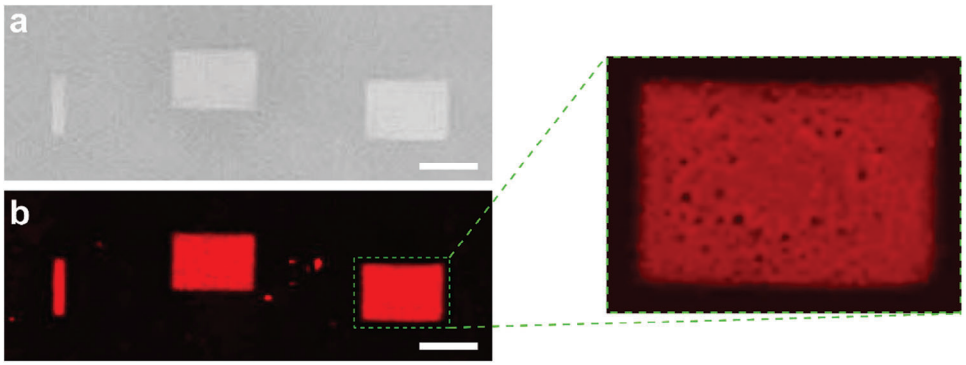

Figure 8. a) 10× magnification bright-field microscopy image (in greyscale) of two crosslinked poly(NIPAAm$_{94}$-*co*-MAA$_5$-*co*-BPQAAm$_1$) polymer pads in the dry state before the post-modification and b) 10× magnification confocal fluorescence microscopy image of the corresponding area in the aqueous state after the post-modification. The narrow crosslinked polymer strip was fabricated and used to ease the navigation/orientation over the sample surface. The size of each pad is 75×50 µm^2. The scale bar is 50 µm. Inset in Figure 8b presents an image of one of the hydrogel pads recorded with a 40× magnification.

© 2024 The Authors. Advanced Functional Materials published by Wiley-VCH GmbH

16163028, 2024, 26, Downloaded from https://onlinelibrary.wiley.com/doi/10.1002/adfm.202315578 by Readcube (Labtiva Inc.), Wiley Online Library on [01/07/2024]. See the Terms and Conditions (https://onlinelibrary.wiley.com/terms-and-conditions) on Wiley Online Library for rules of use; OA articles are governed by the applicable Creative Commons License

wrinkle-patterned topography of collapsed polymer networks was only observed for a specific range of irradiation doses. This characteristic can be beneficial in the context of current interest in wrinkle-pattern engineering of hydrogels.[39–43] In addition, it was shown that a terpolymer poly(NIPAAm-*co*-MAA-*co*-BPQAAm) derived from the best-performing copolymer allows the preparation of thermoresponsive hydrogel structures postmodified with biomolecules. The copolymerization method employed for the synthesis of the photocrosslinkable polymers is a very general approach that can be applied to other types of responsive polymer systems that are prepared by free radical polymerization. As such, the hydrogel networks from multiphoton crosslinking of these polymers can be tailored to respond to other types of stimuli like changes in pH and salt concentrations, to give a few examples.

We believe that the reported approach of multiphoton structuring of thermoresponsive biofunctional hydrogels presented in this publication opens a door for numerous future applications in areas such as externally actuated microstructures serving in micromachines or actively tunable bio-interfaces advancing the performance of bioanalytical technologies. With the use of established multiphoton lithography tools, the reported approach can be adapted for the fabrication of multifunctional 3D nanostructures with higher precision than currently available. The proposed method may offer several advantages with respect to regular approaches using UV-light crosslinking or multiphoton polymerization techniques. For instance, it may allow for the incorporation of cargos (such as a variety of drugs and even viable cells) upon the structure photocrosslinking with a lower risk of their damage. In the same manner, fragile photothermal agents can be coupled with the hydrogel network allowing its spatiotemporal remote control and precise therapy in the biomedical field.[56] Besides, the ability to label with fluorophores and incorporation of biomolecules may allow for the observation and actuating of various microdevices such as responsive hydrogel valves, which can be useful in the lab-on-chip devices[57,58] or be exploited in a new generation of responsive hydrogel-based affinity binding matrices serving in bioanalytical applications. [10]

4. Experimental Section

Chemicals and Working Methods: Benzophenone disulfide (BPdiS) was synthesized as reported elsewhere.[38] For all reactions, the glassware was dried, and the reactions were carried out under an argon atmosphere. Reaction temperatures were either measured in the center of the aluminum block or inside the used oil bath. All solvents were removed with a rotary evaporator under reduced pressure at 40 °C. Products were either dried with lyophilization or with an oil pump at room temperature if not stated otherwise. Water was demineralized by a Millipore filtration system (σ = 18.2 MΩ cm^{-1}) (MilliporeQ, USA). Tetrahydrofuran (99%, VWR, Germany) was dried with potassium and distilled before usage. Dimethylformamide (99.8%, Roth, Germany) was dried with potassium carbonate and distilled under vacuum. Magnesium sulfate (99%. Riedel-de Haën, Germany) was dried at 110 °C before usage. AIBN (98%, Fluka Analytic, Germany) was recrystallized twice from methanol. Triethyl amine (99%, Chemsolute, Germany) was distilled before usage. Methacryloyl chloride (97%, containing up to 15% dimer, Alfa Aesar, Germany) was distilled under vacuum before usage. 1,4-Dioxane (99.5%, Roth, Germany) was dried with sodium and distilled before usage. Acetone (99%), hydrochloric acid (37%), dichloromethane (98%), isopropanol (98%), and methanol (98.5%) were all from VWR Chemicals (Germany). *N*-[3-(dimethylamino)propyl]acrylamide was purchased (98%) from TCI (Japan) and used as received. Methyl-*tert*.-butyl ether (99.5%) was bought from Roth (Germany). Silica 60 (0.063 – 0.2 mm, Macherey-Nagel, Germany) was used for column chromatography. Diethyl ether (99.5%), ethyl acetate (99.8%), methanol (99.8%), *n*-hexane, and chloroform (99.8%) were purchased from Fisher Scientific (UK). All deuterated solvents $CDCl_3$ (99.8%), MeOD (99.8%), and DMSO-*d6* (99.8%) were from Deutero GmbH (Germany). Acetic acid (99.5%) and ethanol (99%) were bought from Chemsolute (Germany). Potassium carbonate (98%) was purchased from Bernd Kraft (Germany). 4-Aminobenzophenone (98%), 4-methylbenzophenone (98%), *N*-bromo succinimide (99%), and acryloyl chloride (96%) were bought from Alfa Aesar (Germany). 2-Amino-3-hydroxy anthraquinone (95%) was bought from ABCR GmbH (Germany).

Monomer Synthesis: BPAm was synthesized based on analogous procedures in the literature.[20,31,32] BPQAAm was synthesized in a two-step synthesis.

Step 1: Bromination of 4-methylbenzophenone was performed according to the literature.[33] Briefly, 4-methylbenzophenone (1.00 g, 5.09 mmol) and AIBN (1 mg, 6.00 µmol) were dissolved in dichloromethane (6 ml) and *N*-bromo succinimide (1.06 g, 5.95 mmol) was added to obtain a dispersion. The reaction was purged with argon for 10 min and refluxed for 21 h at 60 °C afterward. The orange reaction solution was filtered, and the residue was washed with dichloromethane. The solvent was evaporated, and the solid was washed with *n*-hexane. The process was controlled by thin layer chromatography (silica gel, *n*-hexane/ethyl acetate 10:1, *Rf* = 0.59). After evaporating the solvent, the product was washed with water and dried overnight in a vacuum at 60 °C to obtain 1.17 g (4.25 mmol, 84%) of the product. ^{1}H NMR (500 MHz, $CDCl_3$, d/ppm): 4.55 (s, 2 H, CH_2-Br), 7.51-7.84 (m, 9 H, -CH =).^{13}C NMR (125 MHz, $CDCl_3$, d/ppm): 32.3, 126.6, 128.3, 128.9, 130.0, 130.3, 130.5, 132.6, 137.4, 137.5, 142.1, 196.0.

Step 2: 4-(Bromomethyl)benzophenone (400 mg, 1.45 mmol) was dissolved in methyl-*tert*.-butyl ether (19 ml) and *N*-[3-(dimethylamino)propyl]acrylamide (272 mg, 1.75 mmol) dissolved in methyl-*tert*.-butyl ether (2 ml) was added dropwise to the solution. The mixture was stirred for 70 h at room temperature. The solvent was decanted and washed with methyl-*tert*.-butyl ether (6×25 ml) and the solvent was removed by decanting. The white solid was dried in a vacuum overnight, and a yield of 563 mg (1.30 mmol, 90%) was obtained. ^{1}H NMR (500 MHz, $CDCl_3$, d/ppm): 2.29 (m, 2 H, -CH_2-CH_2-CH_2-), 3.26 (s, 6 H, N-$(CH_3)_2$), 3.49 (q, J = 5.56 Hz, 2 H, N-CH_2-CH_2), 3.97 (t, J = 8.11 Hz, 2 H, NH-CH_2), 5.00 (s, 2 H, N$(CH_3)_2$-CH_2-C_{ar}), 5.60 (dd, J = 10.01, 1.43 Hz, 1 H, -CH_2 = CH-), 6.29 (dd, J = 17.17, 1.43 Hz, 1 H, -CH_2 = CH-), 6.47 (dd, J = 16.93, 10.25 Hz, 1 H, -CH_2-CH-), 7.51 (m, 2 H, CH_2-C_{ar}-CH), 7.61 – 7.66 (m, 1 H, -CH = CH_2-), 7.79 (m, 4 H, CH-C_{ar}-C = O), 7.86 (s, 2 H, -CH = CH-), 8.19 (t, J = 5.25 Hz, 1 H, NH). ^{13}C NMR (125 MHz, $CDCl_3$, d/ppm): 23.1, 36.4, 50.0, 63.4, 67.3, 110.0, 126.5, 2×128.7, 130.2, 130.6, 131.2, 2×133.3, 136.8, 139.8, 166.8, 195.8.

AAHAQ was synthesized in reference to the literature.[28,59] In short, AHAQ (250 mg, 1.05 mmol) was dispersed in dry 1,4-dioxane (14 ml). Acryloyl chloride (114 mg, 103 µl, 1.25 mmol) dissolved in dry 1,4-dioxane (2) was added dropwise to the dispersion at 0 °C. After complete addition, the reaction was carried out at 110 °C. The reaction mixture turned from black/red to yellow/green and the progress was controlled by thin-layer chromatography (TLC) (silica gel, EtOAc/toluene 60:40, Rf = 0.63). The solid material was filtered off and washed with 1,4-dioxane (5 ml), before removing the excess of acryloyl chloride under vacuum overnight at 70 °C to obtain a yellow powder as the product with yields up to 85%. ^{1}H NMR (500 MHz, DMSO-d6, d/ppm): 5.81 (dd, J = 11.92, 1.75 Hz, 1 H, -CH = CH_2), 6.34 (m, 1.91 Hz, 1 H, -CH = CH_2), 6.85 (m, 1 H, -CH = CH_2), 7.64 (m, 1 H, -CH = C-OH), 7.84 – 7.93 (m, 2 H, 2x CH_{ar}-C) 8.11 – 8.22 (m, 2 H, 2x ar. -CH =), 9.01 – 9.08 (m, 1 H, CH_{ar}-C-NH), 9.80 (br. s, 1 H, -OH) 11.70 (br. s, 1 H, -NH-). ^{13}C NMR (125 MHz, DMSO-d6, d/ppm): 111.7, 119.1, 125.8, 126.5, 126.6, 127.9, 129.9, 131.6, 132.2, 133.1, 133.3, 134.0, 134.3, 152.5, 164.0, 181.5, 181.8.

© 2024 The Authors. Advanced Functional Materials published by Wiley-VCH GmbH

16163028, 2024, 26, Downloaded from https://onlinelibrary.wiley.com/doi/10.1002/adfm.202315578 by Readcube (Labtiva Inc.), Wiley Online Library on [01/07/2024]. See the Terms and Conditions (https://onlinelibrary.wiley.com/terms-and-conditions) on Wiley Online Library for rules of use; OA articles are governed by the applicable Creative Commons License

16163028, 2024, 26, Downloaded from https://onlinelibrary.wiley.com/doi/10.1002/adfm.202315578 by Readcube (Labtiva Inc.), Wiley Online Library on [01/07/2024]. See the Terms and Conditions (https://onlinelibrary.wiley.com/terms-and-conditions) on Wiley Online Library for rules of use; OA articles are governed by the applicable Creative Commons License

For the synthesis of MAAHAQ, AAHAQ (250 mg, 1.05 mmol) was dispersed in dry 1,4-dioxane (14 ml). Methacryloyl chloride (219.5 mg, 204 µl, 2.10 mmol) dissolved in 1,4-dioxane (2 ml) was added dropwise to the dispersion. The conversion was controlled by TLC (silica gel, toluene/EtOAc 80:20, Rf = 0.37). The reaction suspension turned from black to yellow and a solid precipitated. The solid yellow material was washed with 1,4-dioxane (5 ml), before removing the excess of acryloyl chloride in a vacuum overnight at 60 °C to obtain a red-colored product. ^{1}H NMR (500 MHz, DMSO-d6, d/ppm): 2.01 – 2.04 (m, 3 H, C-CH_3), 5.61 (d, J = 0.95 Hz, 1 H, C-CH_2), 7.64 (s, 1 H, -CH = C-OH), 7.86 – 7.91 (m, 2 H, 2x CH_{ar}-C), 8.16 (m, J = 10.97 Hz, 2 H, 2x ar. -CH =), 9.02 (br. s, 1 H, CH-C_{ar}-NH), 10.64 (br. s, 1 H, CO-NH), 11.76 (br. s, 1 H, -OH). ^{13}C NMR (125 MHz, DMSO-d6, d/ppm): 18.3, 109.8, 111.7, 119.0, 125.8, 125.8, 126.5, 126.6, 130.1, 131.8, 133.2, 134.0, 134.3, 139.6, 152.7, 166.2, 181.4, 181.8.

Copolymer Synthesis: The masses of the various monomers used for the syntheses of the different polymer samples and the polymer characterization data are provided in Table S1 (Supporting Information). NIPAm (99 or 95 mol%), the crosslinker monomer (BPAm, AAHAQ, MAAHAQ, or BPQAAm, 1 or 5 mol%), and AIBN (0.5 ml%) were dissolved in dry 1,4-dioxane (for BPAm), distilled dimethylformamide (for AAHAQ and MAAHAQ), or methanol (for BPQAAm). The mixture was degassed by three freeze-pump-thaw cycles. The polymerization was started by placing the reaction flask in a preheated aluminum block at 65 °C. After 20 h 20 min, the reaction was quenched by cooling with liquid nitrogen and flushing with air. The polymer was precipitated three times in ice-cold diethyl ether (200 ml). The product was lyophilized from 1,4-dioxane. ^{1}H NMR (500 MHz, DMSO-d6, d/ppm) – Poly(NIPAm-*co*-BPAm) (see Figure S8, Supporting Information): 0.85 – 1.15 (CH-$(CH_3)_2$), 1.16 – 1.75 (Backbone, CH_2), 1.75 – 2.20 (backbone, CH), 3.70 – 3.98 (CH-$(CH_3)_2$), 6.88 – 7.48 (C-NH), 7.49 – 7.87 (CH_{ar}), 9.70 – 10.30 (C-NH). Poly(NIPAm-*co*-BPQAAm) (see SI, Figure S9): 0.85 – 1.15 (CH-$(CH_3)_2$), 1.15 – 1.75 (backbone, CH_2), 1.75 – 2.20 (backbone, CH), 2.99 – 3.13 (N-$(CH_3)_2$), 3.70 – 3.95 (CH-$(CH_3)_2$), 6.84 – 7.53 (C-NH) 7.54 – 7.90 (CH_{ar}). Poly(NIPAm-*co*-AAHAQ) (see SI, Figure S10): 0.95 – 1.15 (CH-$(CH_3)_2$), 1.16 – 1.75 (backbone, CH_2), 1.75 – 2.17 (backbone, CH), 3.70 – 3.97 (CH-$(CH_3)_2$), 6.58 – 7.76 (C-NH), 7.79 – 9.20 (CH_{ar}), 11.44 – 11.88 (C-OH). Poly(NIPAm-*co*-MAAHAQ) (see SI, Figure S11): 0.65 – 0.82 (backbone, CH_3), 0.83 – 1.15 (CH-$(CH_3)_2$), 1.16 – 1.75 (backbone, CH_2), 1.75 – 2.20 (backbone, CH), 3.70 – 3.97 (CH-$(CH_3)_2$), 6.58 – 7.76 (C-NH), 7.79 – 9.10 (CH_{ar}), 11.44 – 11.74 (C-OH).

Terpolymer Synthesis: Detailed reaction conditions, yields, and the used amounts are shown in Table S2 (Supporting Information). NIPAm (94 or 90 mol%), MAA (5 mol%), the crosslinker monomer (BPAm, AAHAQ, or BPQAAm, 1 or 5 mol%) and AIBN (0.5 mol%) were dissolved in 3.5 ml of distilled dimethylformamide (for AAHAQ), dry 1,4-dioxane (for BPAm), or methanol (for BPQAAm). The mixture was degassed by three freeze-pump-thaw cycles. The polymerization was initiated by placing the reaction flask in a preheated aluminum block at 65 °C. After 20 h 20 min, the reaction was quenched by cooling with liquid nitrogen and flushing with air. The polymer was precipitated three times in ice-cold diethyl ether (200 ml). The product was freeze-dried from 1,4-dioxane.

^{1}H NMR (500 MHz, DMSO-d6, d/ppm): – Poly($NIPAm_m$-co-MAA_n-co-$AAHAQ_o$): 0.74 – 1.15 (CH-$(CH_3)_2$, backbone-CH_3), 1.16 – 1.75 (backbone, CH_2), 1.75 – 2.20 (backbone, CH), 3.70 – 3.95 (CH-$(CH_3)_2$), 6.65 – 7.75 (C-NH) 7.76 – 9.15 (CH_{ar}), 11.37 – 12.20 (C-OH, COOH). Poly($NIPAm_m$-co-MAA_n-co-$BPAm_o$): 0.75 – 1.15 (CH-$(CH_3)_2$, backbone-CH_3), 1.16 – 1.75 (backbone, CH_2), 1.75 – 2.30 (backbone, CH), 3.70 – 3.95 (CH-$(CH_3)_2$), 6.85 – 7.50 (C-NH), 7.51 – 7.85 (CH_{ar}), 11.75 – 12.05 (-COOH). Poly($NIPAm_m$-co-MAA_n-co-$BPQAAm_o$): 0.70 – 1.22 (CH-$(CH_3)_2$, backbone-CH_3), 1.2 – 1.75 (backbone, CH_2), 1.75 – 2.20 (backbone, CH), 2.99 – 3.10 (N-$(CH_3)_2$), 3.70 – 3.95 (CH-$(CH_3)_2$), 6.85 – 7.54 (C-NH), 7.54 – 8.01 (CH_{ar}), 11.75 – 12.05 (-COOH).

Synthesis of Poly($DMAA_{95}$-co-$AAHAQ_5$): The polymerization of AAHAQ and DMAA was carried out at 75 °C by free radical polymerization in dimethylformamide (DMF) under an inert gas atmosphere. AAHAQ (59.5 mg, 0.203 mmol) and DMAA (384.6 mg, 3.880 mmol) were dissolved in DMF (7 ml). The reaction mixture was degassed by three freeze- and thaw-cycles and initiated by AIBN (3.3 mg, 0.020 mmol). The polymerization was stopped after 24 h by precipitating the reaction mixture in ice-cold diethyl ether. The polymer was purified by dissolving in MeOH and precipitating in ice-cold diethyl ether (2x). The precipitate was separated by centrifugation, dissolved in dioxane (30 ml), and freeze-dried. Yield: 53%, 237.0 mg (M_w = 18.3 kDa, $Đ$ = 2.0). ^{1}H NMR spectrum of poly($DMAA_{95}$-*co*-$AAHAQ_5$) is shown in Figure S24 (see Supporting Information).

Preparation of Sensor Chips: BK7 glass substrates were cut into 25 mm × 25 mm pieces and cleaned with a 1% solution of Hellmanex III in an ultrasound bath. These substrates were either coated with a thin SU-8 or by gold layers. SU-8 coating was prepared from a 100 µL drop of a 2% SU-8 (SU-8 from Micro resist technology GmbH, Germany) dissolved in propylene glycol methyl ether acetate (PGMEA) that was spun at 5000 rpm for 60 s followed by drying in a vacuum oven at 50 °C for 2 h. Gold coatings were prepared by vacuum thermal evaporation (UNIVEX 450, Helmut Heller GmbH, Germany), and 2 nm of chromium and 50 nm of gold were subsequently deposited in a vacuum better than 10^{-6} mbar. The gold-coated substrates were immersed overnight in a 1 mM solution made of the BPdiS linker 3,3′-disulfanediylbis(N-(4-benzoylbenzyl)propanamide dissolved in dimethyl sulfoxide (DMSO, from Sigma–Aldrich, Austria) in order to form a self-assembled monolayer (SAM). The synthesized pNIPAAm and DMAA polymers were dissolved in EtOH at a concentration of 2% (w/w), 150 µL of this solution was spread over the surface of a gold-coated substrate carrying photoactive linker SAM, and it was spun at 2000 rpm for 60 s. After drying overnight in a vacuum oven at 50 °C, the obtained polymer-coated substrates were stored under an Ar atmosphere before the experiments for less than 2 days.

Multiphoton Absorption Lithography Setup: Multiphoton absorption lithography setup was built as schematically shown in Figure S18 (Supporting Information).[60] A compact Er fiber laser (FemtoFiber smart 780, TOptica Photonics) emitting at λ = 785 ± 5 nm with a pulse width of ≈100 fs, a repetition rate of 80 MHz, and a maximum output power of 120 mW was used. The beam was focused on the specimen by a 40× reflective objective (LMM-40X-P01, Thorlabs) and scanned by using a 3D scanning stage (MAX381/M, Thorlabs). The instrument was operated by software developed in LabVIEW 2018 Virtual Instrument (VI) including the in-house developed focus-correction algorithm. The developed VI allowed the authors to move the substrates on the stage in a predefined pattern. It is important to highlight that the effective time-averaged irradiation power, P_L, delivered to the sample surface was significantly lower than the nominal value of the laser (decreased by a factor of 8). This reduction can be attributed to the use of splitters (enabling a combination with a wide-field optical microscope for navigating and focusing the beam at the sample) and due to not using a beam expander for matching the entrance pupil of the microscope objective lens to avoid spreading the pulses due to dispersion.[61,62] Optical images of prepared crosslinked polymer pads in contact with dry and humid air were taken with the help of a bright-field microscope (Olympus BX41, Japan).

Surface Plasmon Resonance Imaging Setup: The schematic of the surface plasmon resonance imaging (SPRi) setup is presented in Figure S28 (Supporting Information). In the setup, light from a superluminescent laser diode with λ_{ex} = 785 nm (iBeam Smart 785S, from TOptica, Photonics AG, Gräfelfing, Germany) was collimated and polarized before being coupled to a high refractive index glass prism (LASFN9, n_p = 1.845). A glass substrate with a 50 nm thin gold layer is optically matched to the prism using a high refractive index oil (Cargille Laboratories, cat. No. 1812; n_o = 1.700) and was mounted on a rotation stage. A flow-cell made of transparent silica cover glass (Sico technology) with drilled inlet and outlet ports and an attached polydimethylsiloxane gasket was clamped onto the sensor chip. The respective flow chamber exhibited a volume of 25 µL. The temperature of the sensor surface was controlled using a Peltier element mounted to the flow-cell through which milliQ water flowed under a constant flow rate (50 µL min^{-1}) using Tygon LMT-55 tubings (Ismatec, Germany) with an inner diameter of 0.25 mm. The intensity of the reflected laser beam was measured by a CCD camera (piA1000-48ag, Basler AG, Germany). The angle of incidence was varied stepwise between 45 and 60° and images were taken at each angular position. The average intensity of the reflected light at the polymer pads (with a size of 50 × 75 $µm^2$) was determined by using the ImageJ program. The average intensity of

© 2024 The Authors. Advanced Functional Materials published by Wiley-VCH GmbH

similar-sized areas above and below the polymer pads was determined as a reference. The intensity of the reference was then subtracted from the intensity of each polymer pad for the given angle of incidence. For the temperature-controlled experiments, the subtracted data were normalized to the data acquired at a temperature of 25 °C.

NMR Spectroscopy: For all NMR spectra, the spectrometer Joel Type ECZ 500 was used. The measurements were performed at room temperature and a Lamor frequency of 500 MHz for the ^{1}H NMR and at 125 MHz for the ^{13}C NMR measurements. Chemical shifts of the signals δ were specified in ppm. The peaks of the non-deuterated solvents were used as an internal standard. The recorded spectra were analyzed with the software ACD/NMR Processor Academic Edition.

Gel Permeation Chromatography: For the determination of the molar mass distribution of all polymers, the SECcurity GPC system Agilent Technologies 1260 infinity instrument was used. A so-called Gram Linear M column, equipped with a 10 µm particle size precolumn was utilized at $T \approx 60$ °C. As eluent, *N*,*N*-dimethylacetamide (DMAc) was used mixed with 1 g L^{-1} LiBr, and 20 µL of the polymer samples were injected. For detection, a UV–vis detector adjusted to 260 nm, as well as an RI detector was used.

UV–vis Spectroscopy: For UV–vis measurements the Epoch 2 microplate reader from BioTek was used.

Atomic Force Microscopy: For topography measurements on pads with dry polymer networks (Figure 2b; Figures S21–S23, Supporting Information), atomic force microscopy (AFM) images were acquired with a Bruker Dimension Icon (Bruker, USA) instrument in tapping mode. For all measurements, triangular sharp silicon nitride SCANASYST-AIR cantilevers (Bruker) with a nominative spring constant of 0.4 N m^{-1}, a resonance frequency of 70 kHz (in the air), and a tip radius of 2 nm were used. Before each experiment, the true spring constant in the air was determined via thermal tune calibration after determining the deflection sensitivity. For the hydrogel stiffness measurements in water (Figure 7), AFM force maps were acquired with a JPK III Nanowizard AFM (Bruker, Germany), mounted on an inverted optical microscope, and equipped with a temperature-controlled liquid sample chamber. For all measurements, triangular sharp silicon nitride MLCT "F" cantilevers (Bruker) with a nominative spring constant of 0.6 N m^{-1}, a resonance frequency of 125 kHz (in the air), and a tip radius of 20 nm were used. Before each experiment, the true spring constant in the air and in liquid was determined via contact-mode calibration. Force maps were acquired with a sampling rate of 25 kHz and 25 µm^{-1} s. Young's modulus was determined by fitting the approach segment of the force curves with an elastic model (Hertz model with Sneddon extension for geometry).

Fluorescence Microscopy: As for the fluorescence observation of the polymer pads, the functional carboxyl groups of the polymer pads were contacted with an aqueous solution of 1-ethyl-3-(3-dimethylami-nopropyl) carbodiimide and *N*-hydroxysuccinimide (200 mM/50 mM) in a petri dish for 20 min. Shortly after rinsing the slide with water, the surface was reacted with AlexaFluor647 anti-human IL-6 antibody (clone MQ2-13A5; cat. number 501 124 from BioLegend, USA) with a mass concentration of 50 µg mL^{-1} in 10 mM sodium acetate buffer (cat. number S8750 from Sigma–Aldrich, Germany) with pH = 5.5 and placed with a cover slide in a humid chamber in the dark for an incubation period of 60 min. Then, the excess IgG molecules were washed off with water and imaged in an aqueous state with a cover slide by a confocal fluorescence microscope (Olympus FV1000).

Supporting Information

Supporting Information is available from the Wiley Online Library or from the author.

Acknowledgements

Y.M.M. was supported by the Austrian Science Fund (FWF) through the Lise Meitner Programme (M 2925). J.D. and S.F. acknowledge support from the European Commission EIC Pathfinder project Versilib (#101046217) and from Czech Science Foundation through the project No. 23-05908K. K.S. and J.D. acknowledge support from Gesellschaft für Forschungsförderung Niederösterreich m.b.H. project LS20-014 ASPIS. Further, the authors thank for the financial support through the BMBF funded Project Medistorplast (13GW0349C) for FD. Financial support for CRVT by the BLE-ptble project PermAFog (854798) is acknowledged. MarvinSketch was used for drawing and displaying chemical structures and reactions (https://www.chemaxon.com).

Open access publishing facilitated by Fyzikalni ustav Akademie ved Ceske republiky, as part of the Wiley - CzechELib agreement.

Conflict of Interest

The authors declare no conflict of interest.

Data Availability Statement

The datasets related to the data presented in the paper can be found under the following link: https://doi.org/10.17605/OSF.IO/YCNJK (Open Science Framework). In the case of interest in some other data, the data can be obtained from the corresponding authors upon request.

Keywords

biofunctional coatings, maskless multiphoton lithography, photocrosslinking, pNIPAAm, thermoresponsive hydrogels

Received: December 6, 2023
Revised: January 18, 2024
Published online: February 22, 2024

[1] M. Heskins, J. E. Guillet, *J. Macromol. Sci. Part A – Chem.* **1968**, *2*, 1441.
[2] S. Dai, P. Ravi, K. C. Tam, *Soft Matter* **2008**, *4*, 435.
[3] D. A. Davis, A. Hamilton, J. Yang, L. D. Cremar, D. Van Gough, S. L. Potisek, M. T. Ong, P. V. Braun, T. J. Martínez, S. R. White, J. S. Moore, N. R. Sottos, *Nature* **2009**, *459*, 68.
[4] Y. L. Colson, M. W. Grinstaff, Y. L. Colson, M. W. Grinstaff, *Adv. Mater.* **2012**, *24*, 3878.
[5] T. Tanaka, I. Nishio, S. T. Sun, S. Ueno-Nishio, *Science (80-.).* **1982**, *218*, 467.
[6] J. Thévenot, H. Oliveira, O. Sandre, S. Lecommandoux, *Chem. Soc. Rev.* **2013**, *42*, 7099.
[7] M. Karimi, P. Sahandi Zangabad, S. Baghaee-Ravari, M. Ghazadeh, H. Mirshekari, M. R. Hamblin, *JACS* **2017**, *139*, 4584.
[8] D. Zhang, B. Ren, Y. Zhang, L. Xu, Q. Huang, Y. He, X. Li, J. Wu, J. Yang, Q. Chen, Y. Chang, J. Zheng, *J. Mater. Chem. B* **2020**, *8*, 3171.
[9] A. Bratek-Skicki, *Appl. Surf. Sci. Adv.* **2021**, *4*, 100068.
[10] F. Diehl, S. Hageneder, S. Fossati, S. K. Auer, J. Dostalek, U. Jonas, *Chem. Soc. Rev.* **2022**, *51*, 3926.
[11] S. Gallagher, L. Florea, K. Fraser, D. Diamond, *Int. J. Mol. Sci.* **2014**, *15*, 5337.
[12] P. Winkler, M. Belitsch, A. Tischler, V. Häfele, H. Ditlbacher, J. R. Krenn, A. Hohenau, M. Nguyen, N. Félidj, C. Mangeney, *Appl. Phys. Lett.* **2015**, *107*, 141906.
[13] S. K. Auer, S. Fossati, Y. Morozov, D. Cattozzo Mor, U. Jonas, J. Dostalek, *J. Phys. Chem. B* **2022**, *126*, 3170.
[14] A. Mourran, H. Zhang, R. Vinokur, M. Möller, *Adv. Mater.* **2017**, *29*, 1604825.
[15] I. Rehor, C. Maslen, P. G. Moerman, B. G. P. van Ravensteijn, R. van Alst, J. Groenewold, H. Burak Eral, W. K. Kegel, *Soft Robot* **2021**, *8*, 10.

© 2024 The Authors. Advanced Functional Materials published by Wiley-VCH GmbH

16163028, 2024, 26, Downloaded from https://onlinelibrary.wiley.com/doi/10.1002/adfm.202315578 by Readcube (Labtiva Inc.), Wiley Online Library on [01/07/2024]. See the Terms and Conditions (https://onlinelibrary.wiley.com/terms-and-conditions) on Wiley Online Library for rules of use; OA articles are governed by the applicable Creative Commons License

[16] J. ter Schiphorst, S. Coleman, J. E. Stumpel, A. Ben Azouz, D. Diamond, A. P. H. J. Schenning, *Chem. Mater.* **2015**, *27*, 5925.
[17] C. Zheng, F. Jin, Y. Zhao, M. Zheng, J. Liu, X. Dong, Z. Xiong, Y. Xia, X. Duan, *Sens. Actuators, B* **2020**, *304*, 127345.
[18] T. Ding, J. Mertens, A. Lombardi, O. A. Scherman, J. J. Baumberg, *ACS Photon* **2017**, *4*, 1453.
[19] Y. Zhao, J. Zhu, W. He, Y. Liu, X. Sang, R. Liu, *Nat. Commun.* **2023**, *14*, 2381.
[20] P. W. Beines, I. Klosterkamp, B. Menges, U. Jonas, W. Knoll, *Langmuir* **2007**, *23*, 2231.
[21] S. Hageneder, V. Jungbluth, R. Soldo, C. Petri, M. Pertiller, M. Kreivi, A. Weinhäusel, U. Jonas, J. Dostalek, *ACS Appl. Mater. Interfaces* **2021**, *13*, 27645.
[22] F. Pirani, N. Sharma, A. Moreno-Cencerrado, S. Fossati, C. Petri, E. Descrovi, J. L. Toca-Herrera, U. Jonas, J. Dostalek, *Macromol. Chem. Phys.* **2017**, *218*, 1600400.
[23] N. Sharma, C. Petri, U. Jonas, J. Dostalek, *Opt. Exp.* **2016**, *24*, 2457.
[24] N. Gisbert Quilis, S. Hageneder, S. Fossati, S. K. Auer, P. Venugopalan, A. Bozdogan, C. Petri, A. Moreno-Cencerrado, J. L. Toca-Herrera, U. Jonas, J. Dostalek, *J. Phys. Chem. C* **2020**, *124*, 3297.
[25] A. Aulasevich, R. F. Roskamp, U. Jonas, B. Menges, J. Dostalek, W. Knoll, *Macromol. Rapid Commun.* **2009**, *30*, 872.
[26] Y. Wang, C.-J. Huang, U. Jonas, T. Wei, J. Dostalek, W. Knoll, *Biosens. Bioelectron.* **2010**, *25*, 1663.
[27] T. G. Jaik, B. Ciubini, F. Frascella, U. Jonas, *Polym. Chem.* **2022**, *13*, 1186.
[28] D. Schwärzle, X. Hou, O. Prucker, J. Rühe, *Adv. Mater.* **2017**, *29*, 1703469.
[29] N. Geid, J. U. Leutner, J. U. Leutner, O. Prucker, J. Rühe, *Actuators* **2023**, *12*, 124.
[30] D. Song, A. Husari, F. Kotz-Helmer, P. Tomakidi, B. E. Rapp, J. Rühe, *Small* **2023**, 2306682, (Early View).
[31] T. Fadida, J.-P. Lellouche, *J. Polym. Res.* **2012**, *19*, 23.
[32] S. Kommeren, J. Dongmo, C. W. M. Bastiaansen, *Soft Matter* **2017**, *13*, 2239.
[33] E. Tayama, H. Kimura, *Angew. Chem., Int. Ed.* **2007**, *46*, 8869.
[34] A. B. Lowe, C. L. McCormick, *Prog. Polym. Sci.* **2007**, *32*, 283.
[35] G. Moad, E. Rizzardo, S. H. Thang, *Aust. J. Chem.* **2005**, *58*, 379.
[36] R. J. Young, P. A. Lovell, *Introduction to Polymers*, CRC Press, Boca Raton **2011**.
[37] N. S. Allen, G. Pullen, M. Edge, I. Weddell, R. Swart, F. Catalina, *J. Photochem. Photobiol. Chem.* **1997**, *109*, 71.
[38] K. Sergelen, C. Petri, U. Jonas, J. Dostalek, *Biointerphases* **2017**, *12*, 051002.
[39] C. M. González-Henríquez, M. A. Sarabia-Vallejos, C. A. Terraza, A. del Campo-García, E. Lopez-Martinez, A. L. Cortajarena, I. Casado-Losada, E. Martínez-Campos, J. Rodríguez-Hernández, *Mater. Sci. Eng. C* **2019**, *97*, 803.
[40] E. Um, Y.-K. Cho, J. Jeong, *ACS Appl. Mater. Interfaces* **2021**, *13*, 15837.
[41] J. Zhang, S. Shen, R. Lin, J. Huang, C. Pu, P. Chen, Q. Duan, X. You, C.g Xu, B. Yan, X. Gao, Z. Shen, L. Cai, X. Qiu, H. Hou, *Adv. Mater.* **2023**, *35*, 2209497.
[42] Y.-A. Lucy Lee, Z. Mousavikhamene, A. Kottaram Amrithanath, S. M. Neidhart, S. Krishnaswamy, G. C. Schatz, T. W. Odom, *Small* **2022**, *18*, 2103865.
[43] C. M. González-Henríquez, G. E. Medel-Molina, F. E. Rodríguez-Umanzor, C. Terraza Inostroza, M. A. Sarabia-Vallejos, J. Rodríguez-Hernández, *Polymer* **2021**, *231*, 124109.
[44] A. V. Ragutkin, M. R. Dasaev, O. V. Kalakutskaya, O. S. Zilova, E. S. Trushin, *Therm. Eng.* **2022**, *69*, 429.
[45] D. Matsukuma, K. Yamamoto, T. Aoyagi, *Langmuir* **2006**, *22*, 5911.
[46] S. K. Christensen, M. C. Chiappelli, R. C. Hayward, *Macromolecules* **2012**, *45*, 5237.
[47] G. Dorman, G. D. Prestwich, *Biochemistry* **1994**, *33*, 5661.
[48] A. A. Lin, V. R. Sastri, G. Tesoro, A. Reiser, R. Eachus, *Macromolecules* **1988**, *21*, 1165.
[49] G. Porter, F. Wilkinson, *Trans. Faraday Soc.* **1961**, *57*, 1686.
[50] G. J. Smets, S. N. El Hamouly, T. J. Oh, *Pure Appl. Chem.* **1984**, *56*, 439.
[51] L. Anhäuser, N. Klöcker, F. Muttach, F. Mäsing, P. Špaček, A. Studer, A. Rentmeister, *Angew. Chem., Int. Ed.* **2020**, *59*, 3161.
[52] Y. Brasse, M. B. Müller, M. Karg, C. Kuttner, T. A. F. König, A. Fery, *ACS Appl. Mater. Interfaces* **2018**, *10*, 3133.
[53] A. N. Bashkatov, E. A. Genina, *Proc. SPIE* **2003**, 5068.
[54] N. Zammatteo, L. Jeanmart, S. Hamels, S. Courtois, P. Louette, L. Hevesi, J. Remacle, *Anal. Biochem.* **2000**, *280*, 143.
[55] H.-N. Chang, S. Sarkar, J. R. Baker, T. B. Norris, *Opt. Mater. Express* **2016**, *6*, 3242.
[56] Y. Qian, S. Lu, J. Meng, W. Chen, J. Li, *Macromol. Biosci.* **2023**, *23*, 2300214.
[57] A. Beck, F. Obst, D. Gruner, A. Voigt, P. Jan Mehner, S. Gruenzner, R. Koerbitz, M. Hadi Shahadha, A. Kutscher, G. Paschew, U. Marschner, A. Richter, *Adv. Mater. Technol.* **2023**, *8*, 2200417.
[58] J. Liu, L. Jiang, A. Liu, S. He, W. Shao, *Sens. Actuators, B* **2022**, *357*, 131434.
[59] N. S. Allen, J. P. Hurley, D. Bannister, G. W. Follows, *Eur. Polym. J.* **1992**, *28*, 1309.
[60] Y. M. Morozov, N. G. Quilis, F. Diehl, S. Klees, J. Grün, U. Jonas, J. Dostalek, *SPIE Proc* **2022**, *12145*, 1214502.
[61] Z. Bor, *Opt. Lett.* **1989**, *14*, 119.
[62] M. Kempe, U. Stamm, B. Wilhelmi, W. Rudolph, *JOSA B* **1992**, *9*, 1158.

© 2024 The Authors. Advanced Functional Materials published by Wiley-VCH GmbH

16163028, 2024, 26, Downloaded from https://onlinelibrary.wiley.com/doi/10.1002/adfm.202315578 by Readcube (Labtiva Inc.), Wiley Online Library on [01/07/2024]. See the Terms and Conditions (https://onlinelibrary.wiley.com/terms-and-conditions) on Wiley Online Library for rules of use; OA articles are governed by the applicable Creative Commons License